

1 **Size-resolved Composition and Morphology of Particulate**
2 **Matter During the Southwest Monsoon in Metro Manila,**
3 **Philippines**
4

5 Melliza Templonuevo Cruz^{1,2}, Paola Angela Bañaga^{1,3}, Grace Betito³, Rachel A. Braun⁴, Connor
6 Stahl⁴, Mojtaba Azadi Aghdam⁴, Maria Obiminda Cambaliza^{1,3}, Hossein Dadashazar⁴, Miguel
7 Ricardo Hilario³, Genevieve Rose Lorenzo¹, Lin Ma⁴, Alexander B. MacDonald⁴, Preciosa
8 Corazon Pabroa⁵, John Robin Yee⁵, James Bernard Simpás^{1,3}, Armin Sorooshian^{4,6}

9
10 ¹Manila Observatory, Quezon City 1101, Philippines

11 ²Institute of Environmental Science and Meteorology, University of the Philippines, Diliman, Quezon City 1101,
12 Philippines

13 ³Department of Physics, School of Science and Engineering, Ateneo de Manila University, Quezon City 1108,
14 Philippines

15 ⁴Department of Chemical and Environmental Engineering, University of Arizona, Tucson, AZ, USA

16 ⁵Philippine Nuclear Research Institute, Commonwealth Avenue, Diliman, Quezon City 1101, Philippines

17 ⁶Department of Hydrology and Atmospheric Sciences, University of Arizona, Tucson, AZ, USA

18
19 *Correspondence to:* Melliza Templonuevo Cruz (liz@observatory.ph)
20

21 **Abstract**

22 This paper presents novel results from size-resolved particulate matter (PM) mass, composition,
23 and morphology measurements conducted during the 2018 Southwest Monsoon (SWM) season in
24 Metro Manila, Philippines. Micro-Orifice Uniform Deposit Impactors (MOUDIs) were used to
25 collect PM sample sets composed of size-resolved measurements at the following aerodynamic
26 cutpoint diameters (D_p): 18, 10, 5.6, 3.2, 1.8, 1.0, 0.56, 0.32, 0.18, 0.10, 0.056 μm . Each sample
27 set was analyzed for composition of the water-soluble fraction. Analysis for mass were done on
28 two sample sets while black carbon (BC) and morphology analysis were done on a single sample
29 set. The bulk of the PM mass was between 0.18–1.0 μm with a dominant mode between 0.32–
30 0.56 μm . Similarly, most of the black carbon (BC) mass was found between 0.10–1.0 μm , peaking
31 between 0.18–0.32 μm . These peaks are located in the Greenfield Gap or the size range between
32 0.10–1.0 μm , where wet scavenging by rain is relatively inefficient. In the range of 0.10 – 0.18
33 μm , BC constituted 78.1% of the measured mass. Comparable contributions of BC (26.9%) and
34 the water-soluble fraction (31.3%) to total PM were observed and most of the unresolved mass,
35 which in total amounted to 41.8%, was for diameters exceeding 0.32 μm . The water-soluble ions
36 and elements exhibited an average combined concentration of 8.53 $\mu\text{g m}^{-3}$, with SO_4^{2-} , NH_4^+ , NO_3^-
37 , Na^+ , and Cl^- as the major contributors. Positive Matrix Factorization (PMF) was applied to
38 identify the possible aerosol sources and estimate their contribution to the water-soluble fraction
39 of collected PM. The factor with the highest contribution was attributed to “Aged” aerosol (48.0%)
40 while “Sea Salt” (22.5%) and “Combustion” emissions (18.7%) had comparable contributions.
41 “Vehicular/Resuspended Dust” (5.6%) as well as “Waste Processing” emissions (5.1%) were also
42 identified. Microscopy analysis highlighted the ubiquity of non-spherical particles regardless of
43 size, which is significant when considering calculations of parameters such as single scattering
44 albedo, asymmetry parameter, and extinction efficiency.

45 The significant influence from Aged aerosol to Metro Manila during the SWM season indicates
46 that local sources in this megacity do not fully govern this coastal area’s aerosol properties. That
47 the majority of the regional aerosol mass burden is accounted for by BC and other insoluble
48 components has important downstream effects on the aerosol hygroscopic properties, which
49 depend on composition. The results are relevant for understanding the impacts of monsoonal
50 features on size-resolved aerosol properties, notably aqueous processing and wet scavenging.
51 Finally, the results of this work provide contextual data for future sampling campaigns in Southeast

52 Asia such as the airborne component of the Cloud, Aerosol, and Monsoon Processes Philippines
53 Experiment (CAMP²Ex) planned for the SWM season in 2019.
54

55 **1. Introduction**

56

57 Ambient atmospheric aerosol particles impact human health, visibility, climate, and the
58 hydrological cycle. Major factors governing these behaviors, such as deposition fraction in the
59 respiratory system and activation into cloud condensation nuclei (CCN), include size and chemical
60 composition. Therefore, size-resolved measurements of ambient aerosol particles can lend
61 additional insights to the behavior and implications of particulate matter (PM) in the atmosphere.
62 One region of interest for characterization of aerosols is Southeast Asia due to increasing
63 urbanization and the exposure of the population to a variety of aerosol sources, both natural and
64 anthropogenic (Hopke et al., 2008). However, use of space-borne remote-sensing instrumentation
65 presents a challenge for characterization of aerosol in this region, due to issues such as varying
66 terrain and cloud cover (Reid et al., 2013).

67 The Philippines represents a country in Southeast Asia with a developing economy, rapid
68 urbanization, old vehicular technology, and less stringent air quality regulations (e.g., Alas et al.,
69 2017). It is also highly sensitive to the effects of climate change including prolonged dry periods
70 and reductions in southwest monsoon (SWM) rainfall in recent decades (e.g., Cruz et al., 2013).
71 Metro Manila is the country's capital and center of political and economic activities. Also referred
72 to as the National Capital Region, Metro Manila is composed of 16 cities and a municipality that
73 collectively occupy a land area of ~619 km². As of 2015, Metro Manila had a population of
74 approximately 12.88 million (Philippine Statistics Authority, 2015). Of the cities comprising the
75 Metro Manila area, the one that is the focus of this study, Quezon City, is the most populated (2.94
76 million people) with a population density of ~17,000 km⁻² as of 2015 (Philippine Statistics
77 Authority, 2015).

78 The rainfall pattern in Southeast Asia is governed by topographic effects and the prevailing
79 surface winds brought by the monsoons. Mountain ranges in the Philippines are generally oriented
80 north to south in the eastern and western coasts. As such, northeasterly winds during the East Asian
81 winter monsoon that starts in November brings wetness (dryness) on the eastern (western) coasts
82 of the country. In contrast, the rainy season starts in May when the Western North Pacific
83 subtropical high moves northeast and the Asian summer monsoon enables the propagation of
84 southwesterly wind through the Philippines (Villafuerte et al., 2014). Metro Manila, located on
85 the western side of the Philippines, therefore experiences wet (May-October) and dry (November-
86 April) seasons. The large seasonal shift in prevailing wind directions can cause changes in the

87 source locations of aerosol transported to the Philippines and the subsequent direction in which
88 emissions from the Philippines are transported, such as to the northwest (e.g., Chuang et al., 2013)
89 or southwest (e.g., Farren et al., 2019). However, one interesting feature of Metro Manila is the
90 consistency of $PM_{2.5}/PM_{10}$ mass concentrations during both the dry ($44/54 \mu\text{g m}^{-3}$) and wet seasons
91 ($43/55 \mu\text{g m}^{-3}$) (Kim Oanh et al., 2006), which stands in contrast to typical assumptions that
92 increased wet scavenging during rainy seasons would lead to decreases in measured PM (e.g., Liao
93 et al., 2006). While similar results are observed in Chennai, India, this behavior is different than
94 other cities in Asia, including Bandung City (Indonesia), Bangkok (Thailand), Beijing (China),
95 and Hanoi City (Vietnam), which exhibit reduced $PM_{2.5}$ levels during the wet season as compared
96 to the dry season (Kim Oanh et al., 2006). While the total PM levels may stay constant across the
97 wet and dry seasons, seasonally-resolved analyses will provide additional insights into how the
98 composition, morphology, and sources (transported vs. local emissions) change on a seasonal
99 basis.

100 Metro Manila has been drawing growing interest for PM research owing to the significant
101 levels of black carbon (BC). A large fraction of PM in Metro Manila can be attributed to BC (e.g.,
102 ~50% of $PM_{2.5}$; Kim Oanh et al., 2006), with previously measured average values of BC at the
103 Manila Observatory (MO) reaching $\sim 10 \mu\text{g m}^{-3}$ for $PM_{2.5}$ (Simpas et al., 2014). The impacts of the
104 high levels of BC present on human health have also received attention (Kecorius et al., 2019).
105 Identified major sources of BC include vehicular, industrial, and cooking emissions (Bautista et
106 al., 2014; Kecorius et al., 2017). Vehicular emissions, especially along roadways where personal
107 cars and motorcycles, commercial trucks, and motorized public transportation, including powered
108 tricycles and *jeepneys*, are plentiful. For instance, measurements of $PM_{2.5}$ at the National Printing
109 Office (NPO) located alongside the major thoroughfare Epifanio de los Santos Avenue (EDSA)
110 were on average $72 \mu\text{g m}^{-3}$; this value is twice the average concentration at MO, an urban mixed
111 site located approximately 5 km from NPO (Simpas et al., 2014). In addition to local emissions,
112 long-range transport of pollution, such as biomass burning, can also impact the study region (e.g.,
113 Xian et al., 2013; Reid et al., 2016a/b). However, most past work referenced above has focused on
114 either total $PM_{2.5}$ or PM_{10} composition, and therefore, detailed size-resolved composition
115 information has been lacking in this region. Like other monsoonal regions (Crosbie et al., 2015;
116 Qu et al., 2015), it is of interest for instance to know if products of aqueous processing (e.g., sulfate,
117 organic acids) during the monsoonal period, promoted by the high humidity, become more

118 prominent in certain size ranges to ultimately enhance hygroscopicity, which is otherwise
119 suppressed with higher BC influence.

120 A year-long sampling campaign (Cloud, Aerosol, and Monsoon Processes Philippines
121 Experiment (CAMP²Ex) weatHER and CompoSition Monitoring (CHECSM) study) was
122 established in July 2018 to collect size-resolved aerosol measurements in Metro Manila. The aim
123 of this study is to report size-resolved PM measurements taken over the course of the SWM (July-
124 October) of 2018 in Quezon City, Metro Manila, Philippines as part of CHECSM. The results of
125 this study are important for the following reasons: (i) they provide size-resolved analysis of BC in
126 an area previously characterized as having one of the highest BC mass percentages in the whole
127 world; (ii) they provide a basis for better understanding the unusual phenomenon of having similar
128 PM levels during a wet and dry season; (iii) they provide contextual data for contrasting with both
129 other coastal megacities and also other monsoonal regions; and (iv) they can lend insights into the
130 characteristics of aerosol transported both into and out of Metro Manila and how important local
131 sources are in Metro Manila relative to transported pollution.

132 Outcomes of this study include (i) the first size-resolved characterization of both aerosol
133 composition and morphology in Metro Manila for the SWM, with implications in terms of PM
134 effects on climate, visibility, the hydrological cycle, and public health owing to the dependence of
135 these impacts on particle size; (ii) archival data that contributes to the timeline of aerosol research
136 in Metro Manila, and more broadly Southeast Asia, where there is considerable concern over air
137 pollution; and (iii) baseline data for aerosol composition to be used to inform and assist research
138 to be conducted during future field campaigns in Southeast Asia including the same seasonal
139 period (i.e., SWM) in 2019 as part of CAMP²Ex, which will involve both surface and airborne
140 measurements.

141 **2. Experimental Methods**

142 **2.1 Sample Site**

143 Sampling was performed at MO in Quezon City, Philippines (14.64° N, 121.08° E). Two
144 MOUDIs were placed inside an unoccupied room on the 3rd floor of the MO administration
145 building (~87 m above sea level). The inlet, located just outside the window, consists of a 2 m
146 long stainless steel tube and a reducer that is connected directly to the MOUDI inlet. Figure 1
147 visually shows the sampling location and potential surrounding aerosol sources. Past work focused

148 on PM_{2.5} suggested that the study location is impacted locally mostly by traffic, various forms of
149 industrial activity, meat cooking from local eateries, and, based on the season, biomass burning
150 (Cohen et al., 2009). This is consistent with another source apportionment study which reported
151 that potential sources in six sites across Metro Manila include traffic, secondary particles, and
152 biomass burning (Kim Oanh et al., 2013).

153 Meteorological data were collected using a Davis Vantage Pro 2 Plus weather station
154 located on the roof (~90 m above sea level, ~15 m above ground level) above where the MOUDIs
155 were located. Except for precipitation, which is reported here as accumulated rainfall, reported
156 values for each meteorological parameter represent averages for the sampling duration of each
157 aerosol measurement. The mean temperature during the periods of MOUDI sample collection
158 ranged from 24.9 to 28.1° C, with accumulated rainfall ranging widely from no rain to up to 78.4
159 mm. To identify sources impacting PM via long-range transport to the Metro Manila region, Figure
160 1a summarizes the five-day back-trajectories for air masses arriving at MO on the days when
161 samples were being collected, calculated using the NOAA Hybrid Single-Particle Lagrangian
162 Integrated Trajectory (HYSPLIT) model (Stein et al., 2015; Rolph, 2016). Trajectory calculations
163 were started at 00, 06, 12, and 18 hours in MO at the height of the MOUDI inlet (~ 12 m above
164 ground level) using meteorological files from the NCEP/NCAR Reanalysis dataset. Trajectory
165 cluster analysis was conducted using TrajStat (Wang et al., 2009). The back-trajectories in Figure
166 1a show that indeed 66% of the wind came from the southwest during the sampling periods.

167 **2.2 MOUDI Sample Sets**

168 PM was collected on Teflon substrates (PTFE membrane, 2 µm pore, 46.2 mm, Whatman)
169 in Micro-Orifice Uniform Deposit Impactors (MOUDI, MSP Corporation, Marple et al., 2014).
170 Size-resolved measurements were taken at the following aerodynamic cutpoint diameters (D_p): 18,
171 10, 5.6, 3.2, 1.8, 1.0, 0.56, 0.32, 0.18, 0.10, 0.056 µm. Fourteen sample sets were collected during
172 the SWM season (July-October 2018), with details about the operational and meteorological
173 conditions during each sample set shown in Table 1. To determine the optimum sampling time that
174 will collect enough sample for subsequent analyses, collection time for the first four samples
175 ranged from 24 to 119 hours. Subsequent sampling were then fixed to 48 hours with one sample
176 set collected every week. The sampling collection was designed to include samples from each day
177 of the week so the collection cycled between Monday – Wednesday, Tuesday – Thursday,

178 Wednesday – Friday, and Saturday – Monday, starting at 1400 (local time) for the weekday
179 samples and 0500 for the weekend samples. The Teflon substrates were pretreated by washing
180 with deionized water and air drying in a covered box. Substrates were placed and retrieved from
181 the cascade impactor inside the laboratory in an adjacent building and transported to and from the
182 sampling site using an impactor holder (Csavina et al., 2011). Samples are immediately placed in
183 the freezer upon retrieval.

184 On two occasions, two pairs of MOUDI sets (Sets MO3/MO4 and MO13/MO14) were
185 collected simultaneously such that one set in each pair could undergo different types of analyses.
186 Sets 3 and 13 underwent gravimetric analysis using a Sartorius ME5-F microbalance. Substrates
187 were conditioned for at least 24 h at a mean temperature of 20-23 °C and a mean relative humidity
188 of 30-40% before pre- and post-weighing (U.S. Environmental Protection Agency, 2016).
189 MOUDI set 13 was additionally examined with a Multi-wavelength Absorption Black Carbon
190 Instrument (MABI; Australian Nuclear Science and Technology Organisation). This optically-
191 based instrument quantifies absorption and mass concentrations at seven wavelengths between 405
192 and 1050 nm; however, results are reported only for 870 nm to be consistent with other studies, as
193 BC is the predominant absorber at that wavelength (e.g., Ramachandran and Rajesh, 2007; Ran et
194 al., 2016). One additional sample set for microscopy analysis was collected for one hour on August
195 1 using aluminum substrates.

196 **2.3 Chemical Composition Analysis**

197 Twelve sample sets, composed of 11 samples each, were analyzed for water-soluble ions
198 and elements (Table 2). In order to preserve samples for additional analysis, each Teflon substrate
199 was cut in half. A half of each substrate was extracted in 8 mL of Milli-Q water (18.2 MΩ-cm)
200 through sonication for 30 min in a sealed polypropylene vial. A blank substrate was processed in
201 the same method to serve as a background control sample. Subsequent chemical analysis of the
202 water-soluble components in the aqueous extracts were performed using ion chromatography (IC;
203 Thermo Scientific Dionex ICS - 2100 system) for the following species: cations = Na⁺, NH₄⁺,
204 Mg²⁺, Ca²⁺, dimethylamine (DMA), trimethylamine (TMA), diethylamine (DEA); anions =,
205 methanesulfonate (MSA), pyruvate, adipate, succinate, maleate, oxalate, phthalate, Cl⁻, NO₃⁻,
206 SO₄²⁻. Owing to co-elution of TMA and DEA in the IC system, a cumulative sum of the two is
207 reported here, which represents an underestimate of their total mass concentration owing to overlap

208 in parts of their peaks. Limits of detection (LOD) were calculated for each species based on their
209 respective calibration curve (Table S1), with LOD being three times the standard deviation of the
210 residuals (predicted signal minus measured signal) divided by the slope of the calibration curve
211 (Miller and Miller, 2018).

212 The aqueous extracts were simultaneously characterized for elemental composition using
213 triple quadrupole inductively coupled plasma mass spectrometry (ICP-QQQ; Agilent 8800 Series)
214 for the following species: K, Al, Fe, Mn, Ti, Ba, Zn, Cu, V, Ni, P, Cr, Co, As, Se, Rb, Sr, Y, Zr,
215 Nb, Mo, Ag, Cd, Sn, Cs, Hf, Tl, Pb. Limits of detection of the examined elements were calculated
216 automatically by the ICP-QQQ instrument and were in the ppt range (Table S1). The sample
217 concentrations represent an average of three separate measurements with a standard deviation of
218 3% or less.

219 Note that some species were detected by both IC and ICP-QQQ (i.e., Na⁺, K⁺, Mg²⁺, Ca²⁺),
220 and that the IC concentrations are used here for all repeated species with the exception of K⁺ owing
221 to better data quality from ICP-QQQ. All IC and ICP-QQQ species concentrations for samples
222 have been corrected by subtracting concentrations from background control samples. For more
223 examples of the application of these methods used for substrate collection and IC/ICP analysis,
224 the reader is referred to other recent work (Braun et al., 2017; Ma et al., 2019; Schlosser et al.,
225 2017).

226 **2.4 Microscopy Analysis**

227 As already noted, one MOUDI set on August 1 was devoted to microscopy analysis.
228 Morphology and additional elemental composition analysis was carried out on this set of aluminum
229 substrates using scanning electron microscopy equipped with energy dispersive X-ray
230 spectroscopy (SEM-EDX) in the Kuiper Imaging cores at the University of Arizona. Secondary
231 electron (SE) imaging and EDX elemental analysis were performed using a Hitachi S-4800 high
232 resolution SEM coupled to a Noran system Six X-ray Microanalysis System by Thermo Fisher
233 Scientific. EDX analysis on individual particles was performed with 30 kV accelerating voltage to
234 obtain weight percentages of individual elements. SEM-EDX results showed that the background
235 control aluminum substrate was dominated by Al (88.27%), with minor contributions from Ag
236 (5.34%), C (4.87%), O (0.79%), Fe (0.67%), and Co (0.05%). Such contributions were manually
237 subtracted from spectra of individual particles on sample substrates, with the remaining elements

238 scaled up to hundred percent. Image processing was conducted with Image J software to measure
239 particle dimensions and adjust the contrast and brightness of images to provide better visualization.

240 **2.5 Computational Analysis**

241 This study reports basic descriptive statistics for chemical concentrations and correlations
242 between different variables. Statistical significance hereafter corresponds to 95% significance
243 based on a two-tailed Student's t-test. To complement correlative analysis for identifying sources
244 of species, positive matrix factorization (PMF) modeling was carried out using the United States
245 Environmental Protection Agency's (US EPA) PMF version 5. A total of 132 samples from the 12
246 sets analyzed for water-soluble ions and elements were used in the PMF analysis. Species
247 concentrations were examined before being inputted to PMF. Species considered as "strong" based
248 on high signal-to-noise ratios ($S/N > 1$) and those with at least 50% of the concentrations above
249 the LOD were used in the PMF modeling (Norris et al., 2014). This resulted in a 132 (samples) \times
250 30 (species) data matrix that was inputted to PMF. Data points with concentrations exceeding the
251 LOD had uncertainty quantified as

252

$$253 \sigma_{ij} = 0.05 \cdot X_{ij} + LOD_{ij}, \quad (\text{Equation 1})$$

254

255 where σ_{ij} , X_{ij} , and LOD_{ij} are the uncertainty, concentration, and LOD, respectively, of the j^{th}
256 species in the i^{th} sample (Reff et al., 2007). When concentration data were not available for a
257 particular stage of a MOUDI set for a species, the geometric mean of the concentrations for that
258 MOUDI stage and species was applied with uncertainty counted as four times the geometric mean
259 value (Polissar et al., 1998; Huang et al., 1999). A 25% extra modeling uncertainty was applied
260 to account for other sources of errors, such as changes in the source profiles and chemical
261 transformations (Dumanoglu et al., 2014; Norris et al., 2014). The model was run 20 times with a
262 randomly chosen starting point for each run.

263 **3. Results**

264 **3.1 Total Mass Concentrations and Charge Balance**

265 The average total mass concentration (\pm standard deviation) of water-soluble species across
266 all MOUDI stages (Table 1) during the study period was $8.53 \pm 4.48 \mu\text{g m}^{-3}$ (range = 2.7–16.6 μg

267 m^{-3}). The species contributing the most to the total water-soluble mass concentration during the
268 SWM included SO_4^{2-} ($44\% \pm 6\%$), NH_4^+ ($18\% \pm 5\%$), NO_3^- ($10 \pm 3\%$), Na^+ ($8 \pm 3\%$), and Cl^- (6%
269 $\pm 3\%$). The meteorological parameters from Table 1 best correlated to total water-soluble mass
270 concentrations were temperature ($r = 0.64$) and rainfall ($r = -0.49$). The highest total mass
271 concentration (set MO13/14 = $16.6 \mu\text{g m}^{-3}$) occurred during the period with one of the highest
272 average temperatures ($27.8 \text{ }^\circ\text{C}$) and second least total rainfall (0.8 mm). Other sampling periods
273 with high mass concentrations (sets MO7, MO8, and MO12) coincided with the highest
274 temperature and lowest rainfall observations. High temperatures, and thus more incident solar
275 radiation, presumably enhanced production of secondary aerosol species via photochemical
276 reactions as has also been observed in other regions for their respective monsoon season (Youn et
277 al., 2013).

278 Low rainfall is thought to have been coincident with reduced wet scavenging of aerosol at
279 the study site as has been demonstrated for other regions such as North America (Tai et al., 2010)
280 and megacities such as Tehran (Crosbie et al., 2014). However, set MO11 exhibited a very low
281 concentration even with high temperature and lack of rainfall, which may be due to changes in the
282 source and transport of aerosol since this sample set coincided with a significant change in average
283 wind direction (290.2° for MO11 vs. $90.1^\circ - 127.5^\circ$ for all other MOUDI sets). While the reported
284 rainfall measurements were taken at MO, inhomogeneous rainfall patterns in the regions
285 surrounding the Philippines could also contribute to the wet scavenging of PM, thereby lowering
286 the quantity of transported particles reaching the sample site. Future work will address the
287 influence of spatiotemporal patterns of precipitation on PM loadings in the Philippines as a point
288 measurement at an aerosol observing site may be misleading.

289 On two occasions, two simultaneous MOUDI sets (Sets MO3/MO4 and MO13/MO14)
290 were collected for the potential to compare different properties that require separate substrates.
291 The total mass concentrations based on gravimetric analysis of sets MO3 and MO13 were $18.6 \mu\text{g}$
292 m^{-3} and $53.0 \mu\text{g m}^{-3}$, respectively (Figure 2). Both sets exhibited a dominant concentration mode
293 between $0.32\text{--}0.56 \mu\text{m}$ and the MO3 set was different in that it exhibited bimodal behavior with a
294 second peak between $1.8\text{--}3.2 \mu\text{m}$. The sum of speciated water-soluble species accounted for only
295 27.8% and 31.3% of the total gravimetric mass of sets MO3 and MO13, respectively, indicative
296 of significant amounts of water-insoluble species undetected by IC and ICP-QQQ. When adding
297 the total mass of BC ($14.3 \mu\text{g m}^{-3}$) to the other resolved species from set MO13 (the one time BC

298 was measured), there was still $22.1 \mu\text{g m}^{-3}$ of unresolved mass (41.8% of total PM). Most of the
299 unaccounted mass was for $D_p > 0.32 \mu\text{m}$.

300 The observation of BC accounting for 26.9% of total PM ($14.3 \mu\text{g m}^{-3}$) is consistent with
301 past work highlighting the significant fraction of BC in the ambient aerosol of Manila (Kim Oanh
302 et al., 2006; Bautista et al., 2014; Simpas et al., 2014; Kecorius et al., 2017). However, this fraction
303 of BC is very high compared to measurements during the monsoon season in other parts of the
304 world. The mass fraction of BC in total suspended PM (TSPM) was 1.6%/2.2% for the monsoon
305 season in 2013/2014 in Kadapa in southern India, even though the TSPM measured was
306 comparable to that in Manila (64.9 and $49.9 \mu\text{g m}^{-3}$, for 2013 and 2014 in Kadapa, respectively)
307 (Begam et al., 2017). Multiple studies during the monsoon season in a coastal region in southwest
308 India showed BC mass contributions of 1.9 – 5% (Aswini et al., 2019 and references therein).
309 Airborne measurements around North America and in Asian outflow revealed that BC accounted
310 for only ~1-2% of $\text{PM}_{1.0}$ (Shingler et al., 2016) and ~5-15% of accumulation mode aerosol mass
311 (Clarke et al., 2004), respectively.

312 To investigate further about the missing species, a charge balance was carried out for all
313 MOUDI sets (Table 2) to compare the sum of charges for cations versus anions based on IC
314 analysis including K from ICP-QQQ analysis (species listed in Section 2.3). The slope of the
315 charge balances (cations on y-axis) for the cumulative dataset was 1.33 and ranged from 0.89 to
316 1.41 for the 12 individual MOUDI sets that had IC and ICP-QQQ analysis conducted on them.
317 Eleven of the 12 sets exhibited slopes above unity indicating that there was a deficit in the amount
318 of anions detected, which presumably included species such as carbonate and various organics. To
319 further determine if there were especially large anion or cation deficits in specific size ranges,
320 slopes are also reported for $0.056\text{--}1 \mu\text{m}$ and $> 1 \mu\text{m}$. There were no obvious differences other than
321 two MOUDI sets exhibited slopes below 1.0 for the smaller diameter range ($0.056\text{--}1 \mu\text{m}$) while
322 all slopes exceeded unity for $> 1 \mu\text{m}$.

323 **3.2 Mass Size Distributions and Morphology**

324 **3.2.1 Black Carbon**

325 The size-resolved nature of BC has not been characterized in Manila and MOUDI set
326 MO13 offered a view into its mass size distribution (Figure 3a). There was a pronounced peak
327 between $0.18\text{--}0.32 \mu\text{m}$ ($5.0 \mu\text{g m}^{-3}$), which is evident visually in the substrate's color when

328 compared to all other stages of that MOUDI set (Figure 3b). This observed peak in the mass size
329 distribution of BC is similar to previous studies of the outflow of East Asian countries (Shiraiwa
330 et al., 2008), biomass burning and urban emissions in Texas (Schwarz et al., 2008), measurements
331 in the Finnish Arctic (Raatikainen et al., 2015), and airborne measurements over Europe
332 (Reddington et al., 2013). In contrast, measurements in Uji, Japan showed a bimodal size
333 distribution for the mass concentration of BC in the submicrometer range (Hitzenberger and
334 Tohno, 2001).

335 In the present study, there were significant amounts of BC extending to as low as the 0.056-
336 0.1 μm MOUDI stage ($0.28 \mu\text{g m}^{-3}$) and extending up in the supermicrometer range with up to
337 $0.25 \mu\text{g m}^{-3}$ measured between 1.8–3.2 μm . Remarkably, BC accounted for approximately 78.1%
338 (51.8%) by mass of the total PM in the range of 0.10 – 0.18 μm (0.18 – 0.32 μm). For comparison,
339 the mass percent contribution of BC measured in the megacity of Nanjing, China was 3.3% (1.6%)
340 at 0.12 (0.08) μm (Ma et al., 2017). Based on visual inspection of color on all MOUDI sets, MO13
341 appears to be representative of the other sets based on the relative intensity of the color black on
342 substrates with different cutpoint diameters (Figure 3b); the 0.18–0.32 μm substrate always was
343 the most black, with varying degrees of blackness extending consistently into the supermicrometer
344 stages.

345 Microscopy analysis revealed evidence of non-spherical particles in each MOUDI stage
346 below 1 μm (Figure 4), which is significant as the common assumption theoretically is that
347 submicrometer particles are typically spherical (e.g., Mielonen et al., 2011). Errors in this
348 assumption impact numerical modeling results and interpretation of remote sensing data for
349 aerosols (e.g., Kahnert et al., 2005), owing to incorrect calculations of parameters such as single
350 scattering albedo, asymmetry parameter, and extinction efficiency (e.g., Mishra et al., 2015). Some
351 studies have noted that submicrometer particles could be composed of an agglomeration of small
352 spherical particles originally formed through gas-to-particle conversion processes (Almeida et al.,
353 2019), which could potentially explain the appearance for some of the observed particles in Figure
354 4. Since only single particles were examined that may not be fully representative of all particles
355 on a particular MOUDI substrate, it is noteworthy that all five particles shown between 0.056 – 1
356 μm were irregularly shaped with signs of both multi-layering and constituents adhered to one
357 another.

358 The images show that a potentially important source of BC in the area could be soot
359 aggregates, which are formed by a vaporization-condensation process during combustion often
360 associated with vehicular exhaust (e.g., Chen et al., 2006; Chithra and Nagendra, 2013; Wu et al.,
361 2017). Kecorius et al. (2017) projected that 94% of total roadside refractory PM with number
362 concentration modes at 20 and 80 nm was linked to *jeepneys*, the most popular and inexpensive
363 mode of public transport in Metro Manila. They associated the larger mode with soot
364 agglomerates, which is consistent with the smallest MOUDI size range examined here (0.056-0.1
365 μm ; Figure 4b) exhibiting signs of agglomeration.

366 The total BC mass concentration integrated across all stages of MOUDI set MO13 (14.3
367 $\mu\text{g m}^{-3}$) was remarkably high in contrast to BC levels measured via either filters, aethalometers, or
368 single particle soot photometers in most other urban regions of the world (Metcalf et al., 2012 and
369 references therein): Los Angeles Basin (airborne: 0.002–0.53 $\mu\text{g m}^{-3}$), Atlanta, Georgia (ground:
370 0.5–3.0 $\mu\text{g m}^{-3}$), Mexico City (airborne: 0.276–1.1 $\mu\text{g m}^{-3}$), Sapporo, Japan (ground: 2.3–8.0 μg
371 m^{-3}), Beijing, China (ground: 6.3–11.1 $\mu\text{g m}^{-3}$), Bangalor, India (ground: 0.4–10.2 $\mu\text{g m}^{-3}$), Paris,
372 France (ground: 7.9 $\mu\text{g m}^{-3}$), Dushanbe, Russia (ground: 4–20 $\mu\text{g m}^{-3}$), Po Valley, Italy (ground:
373 0.5–1.5 $\mu\text{g m}^{-3}$), Thessaloniki, Greece (ground: 3.3–8.9 $\mu\text{g m}^{-3}$). This is intriguing in light of
374 extensive precipitation, and thus wet scavenging of PM, during the study period, which is offset
375 by enormous anthropogenic emissions in the region such as by powered vehicles like the *jeepneys*
376 that are notorious for BC exhaust (Kecorius et al., 2017).

377 A possible explanation for the large contribution of BC to PM, and the persistence of PM
378 after rain events (Kim Oanh et al., 2006), is that the BC is not efficiently scavenged by precipitating
379 rain drops. Small particles enter rain drops via diffusion whereas large particles enter via
380 impaction. However, particles with a diameter in the range of 0.1–1 μm (known as the Greenfield
381 gap) are too large to diffuse efficiently and too small to impact, and are therefore not efficiently
382 scavenged (Seinfeld and Pandis, 2016). Absorption spectroscopy of set MO13 (Figure 2b) reveals
383 that 95% of the BC mass is concentrated in the Greenfield gap, and thus the removal of BC due to
384 precipitation is inefficient. The Greenfield gap contains $62 \pm 11\%$ of the total mass (calculated for
385 MO3/MO13) and $65 \pm 10\%$ of the water-soluble mass (calculated for the other 12 MO sets). As
386 noted earlier, BC observations discussed in this paper were based only on a single MOUDI set and
387 the effect of inefficient scavenging in the Greenfield Gap could just be one of the many potential

388 processes affecting the BC mass size distribution. Subsequent work that will include BC
389 measurements in the dry season will further investigate this hypothesis.

390 **3.2.2 Water-Soluble Ions**

391 There were two characteristic mass size distribution profiles for the water-soluble ions
392 speciated by IC, depending on whether the species were secondarily produced via gas-to-particle
393 conversion or associated with primarily emitted supermicrometer particles. The average IC species
394 mass concentration profile across all MOUDI sets is shown in Figure 5. Secondarily produced
395 species exhibited a mass concentration mode between 0.32–0.56 μm , including common inorganic
396 species (SO_4^{2-} , NH_4^+), MSA, amines (DMA, TMA+DEA), and a suite of organic acids, such as
397 oxalate, phthalate, succinate, and adipate, produced via precursor volatile organic compounds
398 (VOCs). Two organic acids with peaks in other size ranges included maleate (0.56–1 μm) and
399 pyruvate (0.1–0.18 μm). Sources of the inorganics are well documented with SO_4^{2-} and NH_4^+
400 produced by precursor vapors SO_2 and NH_3 , respectively, with ocean-emitted dimethylsulfide
401 (DMS) as an additional precursor to SO_4^{2-} and the primary precursor to MSA.

402 Precursors leading to secondarily-produced alkyl amines such as DMA, TMA, and DEA
403 likely originated from a combination of industrial activity, marine emissions, biomass burning,
404 vehicular activity, sewage treatment, waste incineration, and the food industry (e.g., Facchini et
405 al., 2008; Sorooshian et al., 2009; Ge et al., 2011; VandenBoer et al., 2011); another key source of
406 these species, animal husbandry (Mosier et al., 1973; Schade and Crutzen, 1995; Sorooshian et al.,
407 2008), was ruled out owing to a scarcity of such activity in the study region. Secondarily-produced
408 amine salts likely were formed with SO_4^{2-} as the chief anion owing to its much higher
409 concentrations relative to NO_3^- or organic acids.

410 Dimethylamine was the most abundant amine similar to other marine (Muller et al., 2009)
411 and urban regions (Youn et al., 2015); the average concentration of DMA integrated over all
412 MOUDI stages for all sample sets was 62.2 ng m^{-3} in contrast to 29.8 ng m^{-3} for TMA+DEA. For
413 reference, the other key cation (NH_4^+) participating in salt formation with acids such as H_2SO_4 and
414 HNO_3 was expectedly much more abundant (1.64 $\mu\text{g m}^{-3}$). With regard to the competitive uptake
415 of DMA versus NH_3 in particles, the molar ratio of DMA: NH_4^+ exhibited a unimodal profile
416 between 0.1–1.8 μm with a peak of 0.022 between 0.32–0.56 μm and the lowest values at the tails
417 (0.004 between 0.1–0.18 and 1–1.8 μm); DMA was not above detection limits for either $D_p < 0.1$

418 μm or $D_p > 1.8 \mu\text{m}$. The molar ratios observed were consistent with values measured in urban air
419 of Tucson, Arizona and coastal air in Marina, California (0–0.04; Youn et al., 2015) and near the
420 lower end of the range measured in rural and urban air masses sampled near Toronto (0.005–0.2:
421 VandenBoer et al., 2011).

422 The most abundant organic acid was oxalate ($195 \pm 144 \text{ ng m}^{-3}$), followed by succinate (21
423 $\pm 41 \text{ ng m}^{-3}$), phthalate ($19 \pm 25 \text{ ng m}^{-3}$), maleate ($17 \pm 15 \text{ ng m}^{-3}$), and adipate ($5 \pm 8 \text{ ng m}^{-3}$). The
424 observation of mass concentrations increasing with decreasing carbon number for dicarboxylic
425 acids (i.e., oxalate > succinate > adipate) is consistent with many past studies for other regions as
426 larger chain acids undergo oxidative decay to eventually form oxalate (e.g., Kawamura and
427 Ikushima, 1993; Kawamura and Sakaguchi, 1999; Sorooshian et al., 2007). Maleate is an
428 unsaturated dicarboxylic acid emitted from gas and diesel engines (Rogge et al., 1993) and a
429 product from the photo-oxidation of benzene (Kawamura and Ikushima, 1993). The aromatic
430 dicarboxylic acid phthalate is a known photo-oxidation product of naphthalene and stems largely
431 from plastic processing and fuel combustion (Fraser et al., 2003; Kautzman et al., 2010; Fu et al.,
432 2012; Kleindienst et al., 2012). The oxidation product (MSA) of ocean-derived DMS exhibited an
433 overall average concentration of $11 \pm 7 \text{ ng m}^{-3}$, which is near the lower end of the range of levels
434 reported in other coastal and marine environments (from undetected up to $\sim 200 \text{ ng m}^{-3}$) (e.g.,
435 Saltzman et al., 1983, 1986; Berresheim 1987; Watts et al., 1987; Burgermeister and Georgii,
436 1991; Sorooshian et al., 2015; Xu and Gao, 2015).

437 Water-soluble species exhibiting a peak in the supermicrometer range, usually between
438 $1.8\text{--}5.6 \mu\text{m}$, include those with known affiliations with sea salt (Na^+ , Cl^- , K^+ , Mg^{2+}) and crustal
439 materials such as dust (Ca^{2+}). Nitrate peaked between $1.8\text{--}3.2 \mu\text{m}$, and was best correlated with
440 Na^+ and Mg^{2+} , suggestive of HNO_3 partitioning to sea salt as has been observed in other coastal
441 regions (e.g., Prabhakar et al., 2014a). There was very little NO_3^- in the submicrometer range (0.05
442 $\pm 0.04 \mu\text{g m}^{-3}$) in contrast to supermicrometer sizes ($0.78 \pm 0.47 \mu\text{g m}^{-3}$). More submicrometer
443 NO_3^- in the form of NH_4NO_3 would be expected if there was an excess of NH_3 after neutralizing
444 SO_4^{2-} . The mean ammonium-to-sulfate molar ratio for submicrometer sizes was 2.32 ± 0.52 (range:
445 $1.11 - 2.78$), with full neutralization of SO_4^{2-} in 10 of 12 MOUDI sets. Thus, there was a non-
446 negligible excess in NH_3 that presumably participated in salt formation with HNO_3 and organic
447 species. The significant levels of NO_3^- in the same mode as Na^+ and Cl^- contributed to the
448 significant Cl^- depletion observed, as the mean $\text{Cl}^-:\text{Na}^+$ mass ratio between $1\text{--}10 \mu\text{m}$ (i.e., range of

449 peak sea salt influence) was 0.81 ± 0.28 , which is much lower than the ratio for pure sea salt (1.81)
450 (Martens et al., 1973). The subject of Cl^- depletion in this region will be investigated more
451 thoroughly in subsequent work.

452 Figure 6 shows SEM images of representative single particles in each supermicrometer
453 stage. As would be expected for sea salt and crustal material, most of the particles shown are not
454 spherical. Interestingly, only the particle shown between 1–1.8 μm was close to being spherical.
455 Its composition based on EDX analysis was accounted for mostly by carbon (93.7%) with lower
456 amounts of oxygen (5.8%) and Fe (0.5%). Sea salt particles were found in the next two stages
457 owing to the highest combined weight percentages of Na^+ and Cl^- based on EDX analysis: 1.8–3.2
458 $\mu\text{m} = 36.9\%$; 3.2–5.6 $\mu\text{m} = 46.9\%$. The salt particles are not necessarily cubical but more rounded
459 with signs of agglomeration. These two particles were the only ones among the 11 MOUDI stages
460 exhibiting an EDX signal for S, with contributions amounting to $\sim 2\%$ in each particle. This may
461 be linked to natural SO_4^{2-} existing in sea salt particles. Also, the particle between 3.2–5.6 μm
462 contained a trace amount of Sc (1%). The largest three particles ($\geq 5.6 \mu\text{m}$) were expectedly
463 irregularly shaped with both sharp and rounded edges, comprised mostly of oxygen, Al, Fe, and
464 Ca based on EDX analysis.

465 **3.2.3 Water-Soluble Elements**

466 Averaged data across all MOUDI sets reveal that ICP-QQQ elements exhibited a variety
467 of mass concentration profiles ranging from a distinct mode in either the sub- or supermicrometer
468 range to having multiple modes below and above 1 μm (averages across all MOUDI sets shown
469 in Figure 7). There were several elements with only one distinct peak, being in one of the two
470 stages between 0.18–1.0 μm , including As, Cd, Co, Cr, Cs, Cu, Hf, Mn, Mo, Ni, Rb, Se, Sn, Tl, V,
471 Pb, and Zn. In contrast, the following elements exhibited only one distinct peak in the
472 supermicrometer range: Al, Ba, P, Sr, Ti, Y, and Zr. The rest of the elements exhibited more
473 complex behavior with two distinct peaks in the sub- and supermicrometer range (Ag, Fe, Nb).
474 The following section discusses relationships between all of the ions and elements with a view
475 towards identifying characteristic sources.

476 **3.3 Characteristic Sources and Species Relationships**

477 A combination of PMF and correlation analysis helped identify clusters of closely-related
478 species stemming from distinct sources. The PMF solution with five factors (Figure 8) was chosen
479 because it passed the criteria of physical meaningfulness and it had a calculated ratio of
480 $Q_{\text{true}}:Q_{\text{expected}}$ (1.2) that was very close to the theoretical value of 1.0. There was a high coefficient
481 of determination between measured and predicted mass concentration when summing up all
482 species for each MOUDI stage ($r^2 = 0.79$; sample size, $n = 132$), which added confidence in relying
483 on the PMF model for source apportionment of PM. The five distinct clusters were named for their
484 most plausible sources based on the species included in the groupings, with their overall
485 contributions to the total mass based on PMF analysis shown in parenthesis (Table 3): Aged
486 (48.0%), Sea Salt (22.5%), Combustion (18.7%), Vehicular/Resuspended Dust (5.6%), and Waste
487 Processing (5.1%). For reference, a previous study near the northwestern edge of the Philippines
488 identified six source factors for $PM_{2.5}$ that are fairly similar to those here (Bagtasa et al., 2018):
489 sea salt, resuspended fine dust, local solid waste burning, and long range transport of (i) industrial
490 emissions, (ii) solid waste burning, and (iii) secondary sulfate. Each of our five groupings will be
491 discussed in detail below in decreasing order of contribution to total measured mass
492 concentrations.

493 3.3.1 Aged Aerosol

494 Although not due to one individual source, there was a distinct PMF factor that included
495 species commonly produced via gas-to-particle conversion processes (NH_4^+ , SO_4^{2-} , MSA,
496 oxalate). Correlation analysis (Table 4) also pointed to a large cluster of species significantly
497 related to each other, including the aforementioned ions and a suite of other organic acids
498 (phthalate, succinate, adipate), MSA, and DMA. The latter three inorganic and organic acid ions
499 exhibited significant correlations with each other ($r \geq 0.68$), but also with several elements ($r \geq$
500 0.36: K, V, Rb, Cs, Sn), which were likely co-emitted with the precursor vapors of the secondarily
501 produced ions. Although BC concentrations were quantified from set MO13 only, the results
502 showed that BC was significantly correlated (r : 0.61-0.92) with 15 species, including those
503 mentioned above (owing to co-emission) and also a few elements that were found via PMF to be
504 stronger contributors to the Combustion source discussed in Section 3.3.3 (Ni, Cu, As, Se, Cd, Tl,
505 Pb).

506 This PMF source factor is referred to as Aged Aerosol owing to its characteristic species
507 being linked to secondary particle formation from emissions of local and regional sources.
508 Examples include MSA and DMA being secondarily produced from ocean-derived gaseous
509 emissions (e.g., Sorooshian et al., 2009), and K stemming from biomass burning emissions from
510 upwind regions such as Sumatra and Borneo (Xian et al., 2013). Previous studies (Reid et al., 2012;
511 Wang et al., 2013) have shown that phenomena such as SWM and El-Nino events not only
512 influence biomass burning activities in the Malay Peninsula but also impact the transport and
513 distribution of emissions in the study region. For instance, Reid et al. (2016b) showed that
514 enhancement in monsoonal flow facilitates the advection of biomass burning and anthropogenic
515 emissions to the Philippines from Sumatra and Borneo. Subsequent work will investigate more
516 deeply the impact of biomass burning from those upwind regions on the sample site during the
517 SWM.

518 While NH_4^+ and SO_4^{2-} require time for production owing to being secondarily-produced
519 from precursor vapors (i.e., SO_2 , NH_3), oxalate is the smallest dicarboxylic acid and requires
520 lengthier chemistry pathways for its production and thus is more likely produced in instances of
521 aerosol transport and aging (e.g., Wonaschuetz et al., 2012; Ervens et al., 2018). The various
522 elements associated with this cluster are co-emitted with the precursors to the aforementioned ions
523 and are linked to a variety of sources: metallurgical processes (Anderson et al., 1988; Csavina et
524 al., 2011; Youn et al., 2016), fuel combustion (Nriagu, 1989; Allen et al., 2001; Shafer et al., 2012;
525 Rocha and Correa, 2018), residual oil combustion (Watson et al., 2004), biomass burning (Maudlin
526 et al., 2015), marine and terrestrial biogenic emissions (Sorooshian et al., 2015), and plastics
527 processing (Fraser et al., 2003). In addition, there is extensive ship traffic in the general study
528 region, which is a major source of species in this cluster of species, particularly V and SO_4^{2-} (e.g.,
529 Murphy et al., 2009; Coggon et al., 2012).

530 PMF analysis suggested that the Aged Aerosol factor contributed 48.0% to the total water-
531 soluble mass budget during the study period. Most of the contribution resided in the submicrometer
532 range (68.9%) unlike the supermicrometer range (18.6%), which is consistent with the overall
533 mass size distribution of total PM peaking in the submicrometer range (Figure 2). The
534 reconstructed mass size distribution for this PMF source factor shows the dominance of the mass
535 in the submicrometer range with a peak between 0.32–0.56 μm (Figure 9). The correlation matrices
536 for the sub- and supermicrometer size ranges also show that the correlations between the species

537 most prominent in the Aged Aerosol category are stronger for the former size range (Tables S2-
538 S3). The contribution of this PMF factor to the supermicrometer range is likely associated with
539 species secondarily produced on coarse aerosol such as dust and sea salt. This is evident in the
540 individual species mass size distributions where there is a dominant submicrometer mode but also
541 non-negligible mass above 1 μm .

542 Even though the PM in a heavily populated urban region, such as Metro Manila, is typically
543 thought to be dominated by local sources of aerosols, the current PMF results show that
544 contribution from long range transport is still discernible. This finding is contrary to the
545 expectation that the signal of transported aerosols would be lost in the noise of locally-produced
546 aerosols.

547 3.3.2 Sea Salt

548 As the MO sampling site is approximately 13 km from the nearest shoreline (Figure 1a)
549 and downwind of Manila Bay in the SWM season, there was a great potential for marine emissions
550 to impact the samples. There were several species with similar mass size distributions (mode: 1.8–
551 5.6 μm) and highly correlated total mass concentrations ($r \geq 0.51$) that are linked to sea salt: Cl⁻,
552 Na⁺, Ca²⁺, Mg²⁺, Ba, and Sr. The correlations between these species were stronger when examining
553 just the supermicrometer range as compared to the submicrometer range (Tables S2-S3). The
554 majority of these species was used in PMF analysis and formed a distinct cluster amounting to
555 22.0% of the total study period's mass budget. This source contributed only 0.6% to the
556 submicrometer mass concentration but 53.5% for the supermicrometer size range. The
557 reconstructed mass size distribution for this source factor is shifted farthest to the larger diameters
558 as compared to the other four sources with a peak between 1.8-3.2 μm (Figure 9).

559 It is noteworthy that this factor has the highest share of NO₃⁻ among all identified sources.
560 This result is consistent with mass size distributions shown in Figure 5 in which NO₃⁻ peaks in the
561 supermicrometer range similar to sea salt constituents (e.g., Na⁺ and Cl⁻). Although sea salt
562 particles naturally contain NO₃⁻ (Seinfeld and Pandis, 2016) (mass ratio of NO₃⁻:Na⁺ = 9.8×10^{-8}
563 – 6.5×10^{-5}), the extremely high ratio of NO₃⁻:Na⁺ (mass ratio ~1.8) suggests that only a negligible
564 portion of NO₃⁻ in this factor originated from primary sea salt particles. Thus, the majority of NO₃⁻
565 is most likely due to HNO₃ partitioning to existing sea salt particles (e.g., Fitzgerald, 1991; Allen
566 et al., 1996; Dasgupta et al., 2007; Maudlin et al., 2015). In addition, the Cl⁻:Na⁺ mass ratio in this

567 profile (0.65) is smaller than that in sea salt particles (1.81), indicating high Cl⁻ depletion mainly
568 due to reactions of HNO₃ with NaCl (Ro et al., 2001; Yao et al., 2003; Braun et al., 2017).
569 Moreover, elevated loadings of trace elements (e.g., Ba, Cu, Zn, and Co) could be linked to mixing
570 of marine emissions with urban sources (e.g., vehicle and industrial emissions) during their
571 transport inland to the sampling site (Roth and Okada, 1998). This process of aging is consistent
572 with the observed morphology of the sea salt particles in this study, revealing non-cubical shapes
573 that are rounded owing to the likely addition of acidic species such as HNO₃ (Figure 6).

574 3.3.3 Combustion

575 There are numerous sources of combustion in the study region, including a variety of
576 mobile sources (e.g., cars, utility vehicles, trucks, buses, motorcycles) and stationary sources (e.g.,
577 power stations, cement works, oil refineries, boiler stations, utility boilers). Consequently, the next
578 highest contributor to total mass during the study period according to PMF (18.7%) was the cluster
579 of species including Ni, As, Co, P, Mo, and Cr, which is defined as the Combustion factor. These
580 species have been reported to be rich in particles emitted from combustion of fossil fuel and
581 residual oil (Linak and Miller, 2000; Allen et al., 2001; Wasson et al., 2005; Mahowald et al.,
582 2008; Mooibroek et al., 2011; Prabhakar et al., 2014b). Although not included in PMF analysis,
583 other species significantly correlated with the previous ones include maleate and Ag, which also
584 stem from fuel combustion (Kawamura and Kaplan, 1987; Lin et al., 2005; Sorooshian et al.,
585 2007). Ag specifically is an element in waste incinerator fly ash (Buchholz and Landsberger, 1993;
586 Tsakalou et al., 2018) and its strong correlation with Co ($r = 0.85$) and Mo ($r = 0.64$) provides
587 support for this source factor being linked to combustion processes. Maleate is commonly found
588 in engine exhaust (Kawamura and Kaplan, 1987), while Cr is a tracer for power plant emissions
589 (Singh et al., 2002; Behera et al., 2015). Of all species examined in this study, BC was best
590 correlated with As ($r = 0.92$), while its correlation with Ni ($r = 0.85$) was among the highest.

591 As the elements in this cluster peaked in concentration in the submicrometer mode, the
592 weight percentage of this factor is more than double below 1 μm (23.9%) as compared to above 1
593 μm (11.3%). The reconstructed mass size distribution for this source factor peaks between 0.18–
594 0.32 μm , which is smaller than the modal diameter range for the Aged source factor (0.32–0.56
595 μm) likely owing to closer sources and thus less time for growth to occur via condensation and
596 coagulation.

597 **3.3.4 Vehicular/Resuspended Dust**

598 The next PMF source factor contains chemical signatures of dust because of high
599 contributions to Al, Ti, Ca, and Fe. These crustal elements are strongly related to resuspension of
600 dust by traffic and construction activities (Singh et al., 2002; Harrison et al., 2011). Other elements
601 that were prominent in this factor included Zr, Y, Mn, Cr, and Ba, which are associated with tire
602 and brake wear (Adachi and Tainosho, 2004; Gietl et al., 2010; Song and Gao, 2011; Harrison et
603 al., 2012; Vossler et al., 2016), although some of them can be linked to exhaust as well (e.g., Lin
604 et al., 2005; Song and Gao, 2011). This source is named Vehicular/Resuspended Dust and
605 contributed 5.6% to the total study period's mass concentrations.

606 The weight percentage contribution of this factor was much higher for the supermicrometer
607 range (11.3%) as compared to the submicrometer range (1.5%), which is consistent with the Sea
608 Salt source factor owing to similar mass size distributions of the individual species associated with
609 the two source categories (Figures 5 and 7). Additional species correlated significantly with the
610 crustal species included Hf and Nb, which also exhibited mass peaks between 1.8–3.2 μm . The
611 reconstructed mass size distribution for this source factor is similar to that of Sea Salt in that there
612 is a peak between 1.8–3.2 μm , but there is less of a unimodal profile owing to what appears to be
613 a secondary mode between 0.56–1.0 μm (Figure 9), which could be linked to some of the non-dust
614 components of vehicular emissions.

615 **3.3.5 Waste Processing**

616 The final PMF source factor, contributing the least overall to total mass (5.1%), featured
617 Zn, Cd, Pb, Mn, and Cu as its main components. These species are linked to waste processing,
618 including especially electronic waste (e-waste) and battery burning and recycling (Gullett et al.,
619 2007; Iijima et al., 2007), which was previously reported for Manila (Pabroa et al., 2011). The
620 latter study reported that although there are a few licensed operations for battery recycling, there
621 are numerous unregulated cottage melters across Manila that regularly melt metal from batteries
622 and discard the waste freely. Fujimori et al. (2012) additionally showed that e-waste recycling led
623 to emissions of the following elements (in agreement with this PMF cluster) around Metro Manila:
624 Ni, Cu, Pb, Zn, Cd, Ag, In, As, Co, Fe, and Mn.

625 This was the only PMF factor exhibiting comparable weight percentages both below
626 (5.1%) and above 1 μm (5.3%). This is reflected in the mass size distributions of the species

627 included in this cluster being fairly uniformly distributed below and above 1 μm . This is also
628 demonstrated in the reconstructed mass size distribution of this source factor as it clearly exhibits
629 a mode between the other four sources (0.56–1.0 μm) and is the broadest mode (Figure 9). The
630 explanation for this is likely rooted in the diversity of sources contained within this source profile
631 that lead to different sizes of particles. Examples of such sources include processing of different
632 types of waste at varying temperatures and through various processes (e.g., burning, melting,
633 grinding) (Keshtkar and Ashbaugh, 2007),

634 4. Conclusions

635 This study used various analytical techniques (gravimetry, ion chromatography, triple
636 quadrupole inductively coupled plasma mass spectrometry, black carbon spectroscopy, and
637 microscopy), meteorological data, and a source apportionment model (Positive Matrix
638 Factorization) to characterize the sources, chemical composition, and morphology of size-resolved
639 ambient particulate matter (PM) collected using Micro-Orifice Uniform Deposit Impactors
640 (MOUDIs) in Metro Manila, Philippines during the southwest monsoon (SWM) season of 2018.
641 The main results of this study include the following:

- 642
- 643 • The total mass concentrations were measured on two occasions and were 18.6 $\mu\text{g m}^{-3}$ and 53.0
644 $\mu\text{g m}^{-3}$. Water-soluble mass concentrations were measured on 12 occasions and were on
645 average $8.53 \pm 4.48 \mu\text{g m}^{-3}$ (range = 2.7–16.6 $\mu\text{g m}^{-3}$). Simultaneous measurements of total,
646 water-soluble, and black carbon (BC) mass revealed a composition of 26.9% BC, 31.3% water-
647 soluble components, and 41.8% unaccounted mass.
- 648 • Size-resolved BC mass concentration was measured on one occasion, with the mass sum of all
649 MOUDI stages reaching 14.3 $\mu\text{g m}^{-3}$. Most of the BC mass (95%) was contained in the 0.1–1
650 μm range (i.e., the Greenfield gap) where wet scavenging by rain is relatively inefficient. The
651 measured BC peaked in the size range of 0.18 – 0.32 μm and accounted for 51.8% of the
652 measured PM for that stage. In the range of 0.10 – 0.18 μm , the mass percent contribution of
653 BC to the measured PM was 78.1%.
- 654 • Most of the total mass resided in the submicrometer mode (0.32–0.56 μm); however, one
655 MOUDI set revealed an additional supermicrometer mode (1.8–3.2 μm). Water-soluble
656 species that peaked in the submicrometer mode were associated with secondarily produced

657 species, including inorganic acids, amines, Methanesulfonate (MSA), and organic acids.
658 Water-soluble species that peaked in the supermicrometer mode were associated with sea salt
659 and crustal material. Most of the unaccounted mass was for $D_p > 0.32 \mu\text{m}$.

- 660 • The most abundant water-soluble species was SO_4^{2-} ($44\% \pm 6\%$), followed by NH_4^+ ($18\% \pm$
661 5%), NO_3^- ($10 \pm 3\%$), Na^+ ($8 \pm 3\%$), and Cl^- ($6\% \pm 3\%$). Correlation analysis revealed that
662 total water-soluble mass was most correlated with temperature ($r = 0.64$) and rainfall
663 accumulation ($r = -0.49$) among meteorological factors considered, although other factors were
664 likely influential such as wind direction and speed.
- 665 • Regardless of particle size, the majority of single particles examined with energy dispersive
666 X-ray spectroscopy (SEM-EDX) were non-spherical with evidence of agglomeration.
- 667 • PMF analysis suggested that there were five factors influencing the water-soluble fraction of
668 PM collected at the sampling site. These factors, their contribution to total water-soluble mass,
669 and the main species that permit them to be linked to a physical source are as follows: Aged
670 Aerosol (48.0%; NH_4^+ , SO_4^{2-} , MSA, oxalate), Sea Salt (22.5%; Cl^- , NO_3^- , Ca^{2+} , Na^+ , Mg^{2+} , Ba,
671 Sr), Combustion (18.7%; Ni, As, Co, P, Mo, Cr), Vehicular/Resuspended Dust (5.6%; Al, Ti,
672 Fe), and Waste Processing (5.1%; Zn, Cd, Pb, Mn, Cu). The dominant contribution of Aged
673 aerosols to water-soluble mass contradicts two expectations: (i) locally-produced sources in
674 polluted cities should drown out the signal of transported aerosols, and (ii) the signal of
675 transported aerosols should be significantly reduced due to scavenging processes upwind of
676 the measurement site.

677

678 Although the current study focuses exclusively on the SWM season in Metro Manila,
679 results of this study are applicable to the study of aerosol impacts on Southeast Asia and other
680 regions. First, the detection of Aged aerosols not only from local but also from regional sources
681 confirms previous studies that PM in the region has the ability to travel long distances during the
682 SWM season. Characterization of aerosols in Metro Manila is therefore important for better
683 understanding the impacts that local emissions will have on locations downwind of Metro Manila,
684 including other populated cities in Southeast and East Asia. Transport of pollution and decreased
685 wet scavenging during the SWM season may become increasingly important as studies have shown
686 a decrease in SWM rainfall and increase in the number of no-rain days during the SWM season in
687 the western Philippines in recent decades (e.g., Cruz et al., 2013).

688 Second, Southeast Asia has been named “one of the most hostile environments on the
689 planet for aerosol remote sensing” (Reid et al., 2013). Therefore, space-based remote sensing of
690 aerosol characteristics, such as retrievals of aerosol optical depth (AOD), in this region are
691 difficult. In situ measurements are critical for characterization of PM in this region, especially
692 during seasons such as the SWM when clouds are especially prevalent and remote-sensing
693 retrievals dependent on clear-sky conditions are lacking.

694 Third, this study provides a valuable dataset to compare to other regions impacted by
695 monsoons where the impacts of enhanced moisture and rainfall on size-resolved composition are
696 not well understood. As aqueous processing results in enhanced production of water-soluble
697 species (e.g., sulfate, organic acids), it is noteworthy for this monsoonal region that the water-
698 soluble fraction remains low relative to BC and other insoluble components. This has major
699 implications for the hygroscopicity of the regional PM.

700 Finally, the results of this study will be used to inform future sampling campaigns in this
701 region, including CAMP²Ex planned for the SWM season of 2019 based in the Philippines. As the
702 current MOUDI sampling campaign at the Manila Observatory is expected to extend for a full
703 year, future work will focus on changes in aerosol characteristics and sources on a seasonal basis.

704
705 *Data availability:* All data used in this work are available upon request.

706
707 *Author Contribution:* MTC, MOC, JBS, ABM, CS, and AS designed the experiments and all co-
708 authors carried out some aspect of the data collection. MTC, RAB, CS, LM, HD, and AS conducted
709 data analysis and interpretation. MTC and AS prepared the manuscript with contributions from all
710 co-authors.

711
712 *Competing interests:* The authors declare that they have no conflict of interest.

713
714 *Acknowledgements:* This research was funded by NASA grant 80NSSC18K0148. M. T. Cruz
715 acknowledges support from the Philippine Department of Science and Technology’s ASTHRD
716 Program. R. A. Braun acknowledges support from the ARCS Foundation. A. B. MacDonald
717 acknowledges support from the Mexican National Council for Science and Technology

718 (CONACYT). We acknowledge Agilent Technologies for their support and Shane Snyder's
719 laboratories for ICP-QQQ data.

720

721 **References**

722 Adachi, K., and Tainosho, Y.: Characterization of heavy metal particles embedded in tire dust,
723 *Environ Int*, 30, 1009-1017, 10.1016/j.envint.2004.04.004, 2004.

724

725 Alas, H. D., Müller, T., Birmili, W., Kecorius, S., Cambaliza, M.O., Simpas, J. B., Cayetano, M.,
726 Weinhold, K., Vallar, E., Galvez, M.C., and Wiedensohler, A.: Spatial Characterization of Black
727 Carbon Mass Concentration in the Atmosphere of a Southeast Asian Megacity: An Air Quality
728 Case Study for Metro Manila, Philippines. *Aerosol Air Qual Res.*
729 doi.org/10.4209/aaqr.2017.08.0281, 2017.

730

731 Allen, H. C., Laux, J. M., Vogt, R., FinlaysonPitts, B. J., and Hemminger, J. C.: Water-induced
732 reorganization of ultrathin nitrate films on NaCl: Implications for the tropospheric chemistry of
733 sea salt particles, *J Phys Chem-US*, 100, 6371-6375, DOI 10.1021/jp953675a, 1996.

734

735 Allen, A. G., Nemitz, E., Shi, J. P., Harrison, R. M., and Greenwood, J. C.: Size distributions of
736 trace metals in atmospheric aerosols in the United Kingdom, *Atmos Environ*, 35, 4581-4591, Doi
737 10.1016/S1352-2310(01)00190-X, 2001.

738

739 Almeida, G. P., Bittencourt, A. T., Evangelista, M. S., Vieira-Filho, M. S., and Fornaro, A.:
740 Characterization of aerosol chemical composition from urban pollution in Brazil and its possible
741 impacts on the aerosol hygroscopicity and size distribution, *Atmos Environ*, 202, 149-159,
742 10.1016/j.atmosenv.2019.01.024, 2019.

743

744 Anderson, J. R., Aggett, F. J., Buseck, P. R., Germani, M. S., and Shattuck, T. W.: Chemistry of
745 Individual Aerosol-Particles from Chandler, Arizona, an Arid Urban-Environment, *Environ Sci*
746 *Technol*, 22, 811-818, DOI 10.1021/es00172a011, 1988.

747

748 Aswini, A. R., Hegde, P., Nair, P. R., and Aryasree, S.: Seasonal changes in carbonaceous
749 aerosols over a tropical coastal location in response to meteorological processes, *Science of The*
750 *Total Environment*, 656, 1261-1279, <https://doi.org/10.1016/j.scitotenv.2018.11.366>, 2019.

751

752 Bagtasa, G., Cayetano, M. G., and Yuan, C. S.: Seasonal variation and chemical characterization
753 of PM_{2.5} in northwestern Philippines, *Atmos Chem Phys*, 18, 4965-4980, 10.5194/acp-18-4965-
754 2018, 2018.

755

756 Bautista, A. T., Pabroa, P. C. B., Santos, F. L., Racho, J. M. D., and Quirit, L. L.: Carbonaceous
757 particulate matter characterization in an urban and a rural site in the Philippines, *Atmos Pollut Res*,
758 5, 245-252, 10.5094/Apr.2014.030, 2014.

759

760 Begam, G. R., Vachaspati, C. V., Ahammed, Y. N., Kumar, K. R., Reddy, R. R., Sharma, S. K.,
761 Saxena, M., and Mandal, T. K.: Seasonal characteristics of water-soluble inorganic ions and
762 carbonaceous aerosols in total suspended particulate matter at a rural semi-arid site, Kadapa

763 (India), *Environmental Science and Pollution Research*, 24, 1719-1734, 10.1007/s11356-016-
764 7917-1, 2017.

765

766 Behera, S. N., Betha, R., Huang, X., and Balasubramanian, R.: Characterization and estimation of
767 human airway deposition of size-resolved particulate-bound trace elements during a recent haze
768 episode in Southeast Asia, *Environ Sci Pollut R*, 22, 4265-4280, 10.1007/s11356-014-3645-6,
769 2015.

770

771 Berresheim, H.: Biogenic Sulfur Emissions from the Sub-Antarctic and Antarctic Oceans, *J*
772 *Geophys Res-Atmos*, 92, 13245-13262, 10.1029/JD092iD11p13245, 1987.

773

774 Braun, R. A., Dadashazar, H., MacDonald, A. B., Aldhaif, A. M., Maudlin, L. C., Crosbie, E.,
775 Aghdam, M. A., Mardi, A. H., and Sorooshian, A.: Impact of Wildfire Emissions on Chloride
776 and Bromide Depletion in Marine Aerosol Particles, *Environ Sci Technol*, 51, 9013-9021,
777 10.1021/acs.est.7b02039, 2017.

778

779 Buchholz, B. A., and Landsberger, S.: Trace-Metal Analysis of Size-Fractionated Municipal Solid-
780 Waste Incinerator Fly-Ash and Its Leachates, *J Environ Sci Heal A*, 28, 423-441, Doi
781 10.1080/10934529309375887, 1993.

782

783 Burgermeister, S., and Georgii, H. W.: Distribution of Methanesulfonate, Nss Sulfate and
784 Dimethylsulfide over the Atlantic and the North-Sea, *Atmos Environ a-Gen*, 25, 587-595, Doi
785 10.1016/0960-1686(91)90056-D, 1991.

786

787 Chen, Y. Z., Shah, N., Huggins, F. E., and Huffman, G. P.: Microanalysis of ambient particles
788 from Lexington, KY, by electron microscopy, *Atmos Environ*, 40, 651-663,
789 10.1016/j.atmosenv.2005.09.036, 2006.

790

791 Chithra, V. S., and Nagendra, S. M. S.: Chemical and morphological characteristics of indoor and
792 outdoor particulate matter in an urban environment, *Atmos Environ*, 77, 579-587,
793 10.1016/j.atmosenv.2013.05.044, 2013.

794

795 Chuang, M.-T., Chang, S.-C., Lin, N.-H., Wang, J.-L., Sheu, G.-R., Chang, Y.-J., and Lee, C.-T.:
796 Aerosol chemical properties and related pollutants measured in Dongsha Island in the northern
797 South China Sea during 7-SEAS/Dongsha Experiment, *Atmospheric Environment*, 78, 82-92,
798 <https://doi.org/10.1016/j.atmosenv.2012.05.014>, 2013.

799

800 Clarke, A. D., Shinozuka, Y., Kapustin, V. N., Howell, S., Huebert, B., Doherty, S., Anderson,
801 T., Covert, D., Anderson, J., Hua, X., Moore, K. G., McNaughton, C., Carmichael, G., and
802 Weber, R.: Size distributions and mixtures of dust and black carbon aerosol in Asian outflow:
803 Physiochemistry and optical properties, *J Geophys Res-Atmos*, 109, Artn D15s09
804 10.1029/2003jd004378, 2004.

805

806 Coggon, M. M., Sorooshian, A., Wang, Z., Metcalf, A. R., Frossard, A. A., Lin, J. J., Craven, J.
807 S., Nenes, A., Jonsson, H. H., Russell, L. M., Flagan, R. C., and Seinfeld, J. H.: Ship impacts on
808 the marine atmosphere: insights into the contribution of shipping emissions to the properties of
809 marine aerosol and clouds, *Atmos Chem Phys*, 12, 8439-8458, 10.5194/acp-12-8439-2012, 2012.

810
811 Cohen, D. D., Stelcer, E., Santos, F. L., Prior, M., Thompson, C., and Pabroa, P. C. B.:
812 Fingerprinting and source apportionment of fine particle pollution in Manila by IBA and PMF
813 techniques: A 7-year study, *X-Ray Spectrom*, 38, 18-25, 10.1002/xrs.1112, 2009.
814
815 Crosbie, E., Sorooshian, A., Monfared, N. A., Shingler, T., and Esmaili, O.: A Multi-Year Aerosol
816 Characterization for the Greater Tehran Area Using Satellite, Surface, and Modeling Data,
817 *Atmosphere-Basel*, 5, 178-197, 10.3390/atmos5020178, 2014.
818
819 Crosbie, E., Youn, J. S., Balch, B., Wonaschutz, A., Shingler, T., Wang, Z., Conant, W. C.,
820 Betterton, E. A., and Sorooshian, A.: On the competition among aerosol number, size and
821 composition in predicting CCN variability: a multi-annual field study in an urbanized desert,
822 *Atmos Chem Phys*, 15, 6943-6958, 10.5194/acp-15-6943-2015, 2015.
823
824 Cruz, F. T., Narisma, G. T., Villafuerte, M. Q., Chua, K. U. C., and Olaguera, L. M.: A
825 climatological analysis of the southwest monsoon rainfall in the Philippines, *Atmos Res*, 122, 609-
826 616, 10.1016/j.atmosres.2012.06.010, 2013.
827
828 Csavina, J., Landazuri, A., Wonaschutz, A., Rine, K., Rheinheimer, P., Barbaris, B., Conant, W.,
829 Saez, A. E., and Betterton, E. A.: Metal and Metalloid Contaminants in Atmospheric Aerosols
830 from Mining Operations, *Water Air Soil Poll*, 221, 145-157, 10.1007/s11270-011-0777-x, 2011.
831
832 Dasgupta, P. K., Campbell, S. W., Al-Horr, R. S., Ullah, S. M. R., Li, J. Z., Amalfitano, C., and
833 Poor, N. D.: Conversion of sea salt aerosol to NaNO₃ and the production of HCl: Analysis of
834 temporal behavior of aerosol chloride/nitrate and gaseous HCl/HNO₃ concentrations with
835 AIM, *Atmos Environ*, 41, 4242-4257, 10.1016/j.atmosenv.2006.09.054, 2007.
836
837 Dumanoglu, Y., Kara, M., Altiok, H., Odabasi, M., Elbir, T., and Bayram, A.: Spatial and seasonal
838 variation and source apportionment of volatile organic compounds (VOCs) in a heavily
839 industrialized region, *Atmos Environ*, 98, 168-178, 10.1016/j.atmosenv.2014.08.048, 2014.
840
841 Ervens, B., Sorooshian, A., Aldhaif, A. M., Shingler, T., Crosbie, E., Ziemba, L., Campuzano-
842 Jost, P., Jimenez, J. L., and Wisthaler, A.: Is there an aerosol signature of chemical cloud
843 processing?, *Atmos Chem Phys*, 18, 16099-16119, 10.5194/acp-18-16099-2018, 2018.
844
845 Facchini, M. C., Decesari, S., Rinaldi, M., Carbone, C., Finessi, E., Mircea, M., Fuzzi, S.,
846 Moretti, F., Tagliavini, E., Ceburnis, D., and O'Dowd, C. D.: Important Source of Marine
847 Secondary Organic Aerosol from Biogenic Amines, *Environ Sci Technol*, 42, 9116-9121,
848 10.1021/es8018385, 2008.
849
850 Farren, N. J., Dunmore, R. E., Mead, M. I., Mohd Nadzir, M. S., Samah, A. A., Phang, S. M.,
851 Bandy, B. J., Sturges, W. T., and Hamilton, J. F.: Chemical characterisation of water-soluble
852 ions in atmospheric particulate matter on the east coast of Peninsular Malaysia, *Atmos. Chem.*
853 *Phys.*, 19, 1537-1553, 10.5194/acp-19-1537-2019, 2019.
854
855 Fitzgerald, J. W.: Marine Aerosols - a Review, *Atmos Environ a-Gen*, 25, 533-545, Doi
856 10.1016/0960-1686(91)90050-H, 1991.

857
858 Fraser, M. P., Cass, G. R., and Simoneit, B. R. T.: Air quality model evaluation data for organics.
859 6. C-3-C-24 organic acids, *Environ Sci Technol*, 37, 446-453, 10.1021/es0209262, 2003.
860
861 Fu, P. Q., Kawamura, K., Chen, J., Li, J., Sun, Y. L., Liu, Y., Tachibana, E., Aggarwal, S. G.,
862 Okuzawa, K., Tanimoto, H., Kanaya, Y., and Wang, Z. F.: Diurnal variations of organic
863 molecular tracers and stable carbon isotopic composition in atmospheric aerosols over Mt. Tai in
864 the North China Plain: an influence of biomass burning, *Atmos Chem Phys*, 12, 8359-8375,
865 10.5194/acp-12-8359-2012, 2012.
866
867 Fujimori, T., Takigami, H., Agusa, T., Eguchi, A., Bekki, K., Yoshida, A., Terazono, A., and
868 Ballesteros, F. C.: Impact of metals in surface matrices from formal and informal electronic-
869 waste recycling around Metro Manila, the Philippines, and intra-Asian comparison, *J Hazard*
870 *Mater*, 221-222, 139-146, <https://doi.org/10.1016/j.jhazmat.2012.04.019>, 2012.
871
872 Ge, X. L., Wexler, A. S., and Clegg, S. L.: Atmospheric amines - Part I. A review, *Atmos Environ*,
873 45, 524-546, 10.1016/j.atmosenv.2010.10.012, 2011.
874
875 Gietl, J. K., Lawrence, R., Thorpe, A. J., and Harrison, R. M.: Identification of brake wear particles
876 and derivation of a quantitative tracer for brake dust at a major road, *Atmos Environ*, 44, 141-146,
877 10.1016/j.atmosenv.2009.10.016, 2010.
878
879 Gullett, B. K., Linak, W. P., Touati, A., Wasson, S. J., Gatica, S., and King, C. J.: Characterization
880 of air emissions and residual ash from open burning of electronic wastes during simulated
881 rudimentary recycling operations, *J Mater Cycles Waste*, 9, 69-79, 10.1007/s10163-006-0161-x,
882 2007.
883
884 Harrison, R. M., Beddows, D. C. S., and Dall'Osto, M.: PMF Analysis of Wide-Range Particle
885 Size Spectra Collected on a Major Highway, *Environ Sci Technol*, 45, 5522-5528,
886 10.1021/es2006622, 2011.
887
888 Harrison, R. M., Jones, A. M., Gietl, J., Yin, J. X., and Green, D. C.: Estimation of the
889 Contributions of Brake Dust, Tire Wear, and Resuspension to Nonexhaust Traffic Particles
890 Derived from Atmospheric Measurements, *Environ Sci Technol*, 46, 6523-6529,
891 10.1021/es300894r, 2012.
892
893 Hitzenberger, R., and Tohno, S.: Comparison of black carbon (BC) aerosols in two urban areas –
894 concentrations and size distributions, *Atmospheric Environment*, 35, 2153-2167,
895 [https://doi.org/10.1016/S1352-2310\(00\)00480-5](https://doi.org/10.1016/S1352-2310(00)00480-5), 2001.
896
897 Hopke, P. K., Cohen, D. D., Begum, B. A., Biswas, S. K., Ni, B., Pandit, G. G., Santoso, M.,
898 Chung, Y. S., Davy, P., Markwitz, A., Waheed, S., Siddique, N., Santos, F. L., Pabroa, P. C. B.,
899 Seneviratne, M. C. S., Wimolwattanapun, W., Bunprapob, S., Vuong, T. B., Duy Hien, P. and
900 Markowicz, A.: Urban air quality in the Asian region, *Sci. Total Environ.*, 404(1), 103–112,
901 doi:10.1016/j.scitotenv.2008.05.039, 2008.
902

903 Huang, S. L., Rahn, K. A., and Arimoto, R.: Testing and optimizing two factor-analysis techniques
904 on aerosol at Narragansett, Rhode Island, *Atmos Environ*, 33, 2169-2185, Doi 10.1016/S1352-
905 2310(98)00324-0, 1999.

906

907 Iijima, A., Sato, K., Yano, K., Tago, H., Kato, M., Kimura, H., and Furuta, N.: Particle size and
908 composition distribution analysis of automotive brake abrasion dusts for the evaluation of
909 antimony sources of airborne particulate matter, *Atmos Environ*, 41, 4908-4919,
910 10.1016/j.atmosenv.2007.02.005, 2007.

911

912 Kahnert, M., Nousiainen, T., and Veihelmann, B.: Spherical and spheroidal model particles as an
913 error source in aerosol climate forcing and radiance computations: A case study for feldspar
914 aerosols, *J Geophys Res-Atmos*, 110, Artn D18s13, 10.1029/2004jd005558, 2005.

915

916 Kautzman, K. E., Surratt, J. D., Chan, M. N., Chan, A. W. H., Hersey, S. P., Chhabra, P. S.,
917 Dalleska, N. F., Wennberg, P. O., Flagan, R. C., and Seinfeld, J. H.: Chemical Composition of
918 Gas- and Aerosol-Phase Products from the Photooxidation of Naphthalene, *J Phys Chem A*, 114,
919 913-934, 10.1021/jp908530s, 2010.

920

921 Kawamura, K., and Ikushima, K.: Seasonal-Changes in the Distribution of Dicarboxylic-Acids in
922 the Urban Atmosphere, *Environ Sci Technol*, 27, 2227-2235, DOI 10.1021/es00047a033, 1993.

923

924 Kawamura, K., and Kaplan, I. R.: Motor Exhaust Emissions as a Primary Source for Dicarboxylic-
925 Acids in Los-Angeles Ambient Air, *Environ Sci Technol*, 21, 105-110, DOI
926 10.1021/es00155a014, 1987.

927

928 Kawamura, K., and Sakaguchi, F.: Molecular distributions of water soluble dicarboxylic acids in
929 marine aerosols over the Pacific Ocean including tropics, *J Geophys Res-Atmos*, 104, 3501-3509,
930 Doi 10.1029/1998jd100041, 1999.

931

932 Kecorius, S., Madueño, L., Löndahl, J., Vallar, E., Galvez, M. C., Idolor, L. F., Gonzaga-
933 Cayetano, M., Müller, T., Birmili, W., and Wiedensohler, A.: Respiratory tract deposition of
934 inhaled roadside ultrafine refractory particles in a polluted megacity of South-East Asia, *Science*
935 *of The Total Environment*, 663, 265-274, <https://doi.org/10.1016/j.scitotenv.2019.01.338>, 2019.

936

937 Kecorius, S., Madueno, L., Vallar, E., Alas, H., Betito, G., Birmili, W., Cambaliza, M. O., Catipay,
938 G., Gonzaga-Cayetano, M., Galvez, M. C., Lorenzo, G., Muller, T., Simpas, J. B., Tamayo, E. G.,
939 and Wiedensohler, A.: Aerosol particle mixing state, refractory particle number size distributions
940 and emission factors in a polluted urban environment: Case study of Metro Manila, Philippines,
941 *Atmos Environ*, 170, 169-183, 10.1016/j.atmosenv.2017.09.037, 2017.

942

943 Keshtkar, H., and Ashbaugh, L. L.: Size distribution of polycyclic aromatic hydrocarbon
944 particulate emission factors from agricultural burning, *Atmos Environ*, 41, 2729-2739,
945 10.1016/j.atmosenv.2006.11.043, 2007.

946

947 Kim Oanh, N. T., Upadhyay, N., Zhuang, Y. H., Hao, Z. P., Murthy, D. V. S., Lestari, P., Villarin,
948 J. T., Chengchua, K., Co, H. X., Dung, N. T. and Lindgren, E. S.: Particulate air pollution in six

949 Asian cities: Spatial and temporal distributions, and associated sources, *Atmos. Environ.*, 40(18),
950 3367–3380, doi:10.1016/j.atmosenv.2006.01.050, 2006.
951
952 Kim Oanh, N. T., Pongkiatkul, P., Cruz, M. T., Trung Dung, N., Phillip, L., Zhang, G., and Lestari,
953 P.: Monitoring and Source Apportionment for Particulate Matter Pollution in Six Asian Cities, in:
954 Integrated Air Quality Management: Asian Case Studies, Kim Oanh, N. T. (Ed.), CRC Press,
955 Taylor & Francis Group, USA, 97-124, 2013.
956 Kleindienst, T. E., Jaoui, M., Lewandowski, M., Offenber, J. H., and Docherty, K. S.: The
957 formation of SOA and chemical tracer compounds from the photooxidation of naphthalene and its
958 methyl analogs in the presence and absence of nitrogen oxides, *Atmos Chem Phys*, 12, 8711-8726,
959 10.5194/acp-12-8711-2012, 2012.
960
961 Liao, H., Chen, W. T., and Seinfeld, J. H.: Role of climate change in global predictions of future
962 tropospheric ozone and aerosols, *J Geophys Res-Atmos*, 111, Artn D12304,
963 10.1029/2005jd006852, 2006.
964
965 Lin, C. C., Chen, S. J., Huang, K. L., Hwang, W. I., Chang-Chien, G. P., and Lin, W. Y.:
966 Characteristics of metals in nano/ultrafine/fine/coarse particles collected beside a heavily
967 trafficked road, *Environ Sci Technol*, 39, 8113-8122, 10.1021/es048182a, 2005.
968
969 Linak, W. P., and Miller, C. A.: Comparison of particle size distributions and elemental
970 partitioning from the combustion of pulverized coal and residual fuel oil, *J Air Waste Manage*, 50,
971 1532-1544, Doi 10.1080/10473289.2000.10464171, 2000.
972
973 Ma, Y., Li, S., Zheng, J., Khalizov, A., Wang, X., Wang, Z., and Zhou, Y.: Size-resolved
974 measurements of mixing state and cloud-nucleating ability of aerosols in Nanjing, China, *Journal*
975 *of Geophysical Research: Atmospheres*, 122, 9430-9450, 10.1002/2017jd026583, 2017.
976
977 Ma, L., Dadashazar, D., Braun, R. A., MacDonald, A. B., Aghdam, M. A., Maudlin, L. C., and
978 Sorooshian, A.: Size-resolved characteristics of water-soluble particulate elements in a coastal
979 area: Source identification, influence of wildfires, and diurnal variability, *Atmos. Environ.*, 206,
980 72-84, <https://doi.org/10.1016/j.atmosenv.2019.02.045>, 2019.
981
982 Mahowald, N., Jickells, T. D., Baker, A. R., Artaxo, P., Benitez-Nelson, C. R., Bergametti, G.,
983 Bond, T. C., Chen, Y., Cohen, D. D., Herut, B., Kubilay, N., Losno, R., Luo, C., Maenhaut, W.,
984 McGee, K. A., Okin, G. S., Siefert, R. L., and Tsukuda, S.: Global distribution of atmospheric
985 phosphorus sources, concentrations and deposition rates, and anthropogenic impacts, *Global*
986 *Biogeochem Cy*, 22, 10.1029/2008gb003240, 2008.
987
988 Marple, V., Olson, B., Romay, F., Hudak, G., Geerts, S. M. and Lundgren, D.: Second generation
989 micro-orifice uniform deposit impactor, 120 MOUDI-II: Design, Evaluation, and application to
990 long-term ambient sampling, *Aerosol Sci. Technol.*, 48(4), 427–433,
991 doi:10.1080/02786826.2014.884274, 2014.
992

993 Martens, C. S., Wesolowski, J. J., Harriss, R. C., and Kaifer, R.: Chlorine Loss from Puerto-Rican
994 and San-Francisco-Bay Area Marine Aerosols, *J Geophys Res*, 78, 8778-8792, DOI
995 10.1029/JC078i036p08778, 1973.
996
997 Maudlin, L. C., Wang, Z., Jonsson, H. H., and Sorooshian, A.: Impact of wildfires on size-
998 resolved aerosol composition at a coastal California site, *Atmos Environ*, 119, 59-68,
999 10.1016/j.atmosenv.2015.08.039, 2015.
1000
1001 Metcalf, A. R., Craven, J. S., Ensberg, J. J., Brioude, J., Angevine, W., Sorooshian, A., Duong,
1002 H. T., Jonsson, H. H., Flagan, R. C., and Seinfeld, J. H.: Black carbon aerosol over the Los
1003 Angeles Basin during CalNex, *J Geophys Res-Atmos*, 117, 10.1029/2011jd017255, 2012.
1004
1005 Mielonen, T., Levy, R. C., Aaltonen, V., Komppula, M., de Leeuw, G., Huttunen, J., Lihavainen,
1006 H., Kolmonen, P., Lehtinen, K. E. J., and Arola, A.: Evaluating the assumptions of surface
1007 reflectance and aerosol type selection within the MODIS aerosol retrieval over land: the problem
1008 of dust type selection, *Atmos Meas Tech*, 4, 201-214, 10.5194/amt-4-201-2011, 2011.
1009
1010 Miller, J., and Miller, J.C.: *Statistics and chemometrics for analytical chemistry*. Pearson
1011 Education, 2018.
1012
1013 Mishra, S. K., Agnihotri, R., Yadav, P. K., Singh, S., Prasad, M. V. S. N., Praveen, P. S., Tawale,
1014 J. S., Rashmi, Mishra, N. D., Arya, B. C., and Sharma, C.: Morphology of Atmospheric Particles
1015 over Semi-Arid Region (Jaipur, Rajasthan) of India: Implications for Optical Properties, *Aerosol*
1016 *Air Qual Res*, 15, 974-+, 10.4209/aaqr.2014.10.0244, 2015.
1017
1018 Mooibroek, D., Schaap, M., Weijers, E. P., and Hoogerbrugge, R.: Source apportionment and
1019 spatial variability of PM_{2.5} using measurements at five sites in the Netherlands, *Atmospheric*
1020 *Environment*, 45, 4180-4191, 10.1016/j.atmosenv.2011.05.017, 2011.
1021
1022 Mosier, A. R., Andre, C. E., and Viets, F. G.: Identification of Aliphatic-Amines Volatilized from
1023 Cattle Feedyard, *Environ Sci Technol*, 7, 642-644, DOI 10.1021/es60079a009, 1973.
1024
1025 Muller, C., Iinuma, Y., Karstensen, J., van Pinxteren, D., Lehmann, S., Gnauk, T., and Herrmann,
1026 H.: Seasonal variation of aliphatic amines in marine sub-micrometer particles at the Cape Verde
1027 islands, *Atmos Chem Phys*, 9, 9587-9597, 2009.
1028
1029 Murphy, S. M., Agrawal, H., Sorooshian, A., Padro, L. T., Gates, H., Hersey, S., Welch, W. A.,
1030 Jung, H., Miller, J. W., Cocker, D. R., Nenes, A., Jonsson, H. H., Flagan, R. C., and Seinfeld, J.
1031 H.: Comprehensive Simultaneous Shipboard and Airborne Characterization of Exhaust from a
1032 Modern Container Ship at Sea, *Environ Sci Technol*, 43, 4626-4640, 10.1021/es802413j, 2009.
1033
1034 Norris, G., Duvall, R., Brown, S., and Bai, S.: *EPA Positive Matrix Factorization (PMF) 5.0*
1035 *fundamentals and User Guide Prepared for the US Environmental Protection Agency Office of*
1036 *Research and Development, Washington, DC. Inc., Petaluma, 2014.*
1037
1038 Nriagu, J. O.: A Global Assessment of Natural Sources of Atmospheric Trace-Metals, *Nature*, 338,
1039 47-49, DOI 10.1038/338047a0, 1989.

1040
1041 Pabroa, P. C. B., Santos, F. L., Morco, R. P., Racho, J. M. D., Bautista, A. T., and Bucal, C. G. D.:
1042 Receptor modeling studies for the characterization of air particulate lead pollution sources in
1043 Valenzuela sampling site (Philippines), *Atmos Pollut Res*, 2, 213-218, 10.5094/Apr.2011.027,
1044 2011.
1045
1046 Philippine Statistics Authority: <https://psa.gov.ph/>, Accessed 28 August 2018.
1047
1048 Polissar, A., Hopke, P., Paatero, P., Malm, W., and Sisler, J.: Atmospheric aerosol over Alaska 2.
1049 Elemental composition and sources. *Journal of Geophysical Research* 103, 19045-19057, 1998.
1050
1051 Prabhakar, G., Ervens, B., Wang, Z., Maudlin, L. C., Coggon, M. M., Jonsson, H. H., Seinfeld, J.
1052 H., and Sorooshian, A.: Sources of nitrate in stratocumulus cloud water: Airborne measurements
1053 during the 2011 E-PEACE and 2013 NiCE studies, *Atmos Environ*, 97, 166-173,
1054 10.1016/j.atmosenv.2014.08.019, 2014a.
1055
1056 Prabhakar, G., Sorooshian, A., Toffol, E., Arellano, A. F., and Betterton, E. A.: Spatiotemporal
1057 distribution of airborne particulate metals and metalloids in a populated arid region, *Atmos*
1058 *Environ*, 92, 339-347, 10.1016/j.atmosenv.2014.04.044, 2014b.
1059
1060 Qu, W. J., Wang, J., Zhang, X. Y., Wang, D., and Sheng, L. F.: Influence of relative humidity on
1061 aerosol composition: Impacts on light extinction and visibility impairment at two sites in coastal
1062 area of China, *Atmos Res*, 153, 500-511, 10.1016/j.atmosres.2014.10.009, 2015.
1063
1064 Raatikainen, T., Brus, D., Hyvärinen, A. P., Svensson, J., Asmi, E., and Lihavainen, H.: Black
1065 carbon concentrations and mixing state in the Finnish Arctic, *Atmos. Chem. Phys.*, 15, 10057-
1066 10070, 10.5194/acp-15-10057-2015, 2015.
1067
1068 Ramachandran, S., and Rajesh, T. A.: Black carbon aerosol mass concentrations over
1069 Ahmedabad, an urban location in western India: Comparison with urban sites in Asia, Europe,
1070 Canada, and the United States, *J Geophys Res-Atmos*, 112, 10.1029/2006jd007488, 2007.
1071
1072 Ran, L., Deng, Z. Z., Wang, P. C., and Xia, X. A.: Black carbon and wavelength-dependent aerosol
1073 absorption in the North China Plain based on two-year aethalometer measurements, *Atmos*
1074 *Environ*, 142, 132-144, 10.1016/j.atmosenv.2016.07.014, 2016.
1075
1076 Reddington, C. L., McMeeking, G., Mann, G. W., Coe, H., Frontoso, M. G., Liu, D., Flynn, M.,
1077 Spracklen, D. V., and Carslaw, K. S.: The mass and number size distributions of black carbon
1078 aerosol over Europe, *Atmos. Chem. Phys.*, 13, 4917-4939, 10.5194/acp-13-4917-2013, 2013.
1079
1080 Reff, A., Eberly, S.I., and Bhave, P.V.: Receptor modeling of ambient particulate matter data using
1081 positive matrix factorization: Review of existing methods. *J Air Waste Manage* 57, 146-154, 2007.
1082
1083 Reid, J. S., Xian, P., Hyer, E. J., Flatau, M. K., Ramirez, E. M., Turk, F. J., Sampson, C. R., Zhang,
1084 C., Fukada, E. M., and Maloney, E. D.: Multi-scale meteorological conceptual analysis of observed
1085 active fire hotspot activity and smoke optical depth in the Maritime Continent, *Atmos Chem Phys*,
1086 12, 2117-2147, 10.5194/acp-12-2117-2012, 2012.

1087

1088 Reid, J. S., Hyer, E. J., Johnson, R. S., Holben, B. N., Yokelson, R. J., Zhang, J. L., Campbell, J.
 1089 R., Christopher, S. A., Di Girolamo, L., Giglio, L., Holz, R. E., Kearney, C., Miettinen, J., Reid,
 1090 E. A., Turk, F. J., Wang, J., Xian, P., Zhao, G. Y., Balasubramanian, R., Chew, B. N., Janjai, S.,
 1091 Lagrosas, N., Lestari, P., Lin, N. H., Mahmud, M., Nguyen, A. X., Norris, B., Oanh, N. T. K., Oo,
 1092 M., Salinas, S. V., Welton, E. J., and Liew, S. C.: Observing and understanding the Southeast
 1093 Asian aerosol system by remote sensing: An initial review and analysis for the Seven Southeast
 1094 Asian Studies (7SEAS) program, *Atmos Res*, 122, 403-468, 10.1016/j.atmosres.2012.06.005,
 1095 2013.

1096

1097 Reid, J. S., Xian, P., Holben, B. N., Hyer, E. J., Reid, E. A., Salinas, S. V., Zhang, J. L., Campbell,
 1098 J. R., Chew, B. N., Holz, R. E., Kuciauskas, A. P., Lagrosas, N., Posselt, D. J., Sampson, C. R.,
 1099 Walker, A. L., Welton, E. J., and Zhang, C. D.: Aerosol meteorology of the Maritime Continent
 1100 for the 2012 7SEAS southwest monsoon intensive study - Part 1: regional-scale phenomena,
 1101 *Atmos Chem Phys*, 16, 14041-14056, 10.5194/acp-16-14041-2016, 2016a.

1102

1103 Reid, J. S., Lagrosas, N. D., Jonsson, H. H., Reid, E. A., Atwood, S. A., Boyd, T. J., Ghate, V. P.,
 1104 Xian, P., Posselt, D. J., Simpas, J. B., Uy, S. N., Zaiger, K., Blake, D. R., Bucholtz, A., Campbell,
 1105 J. R., Chew, B. N., Cliff, S. S., Holben, B. N., Holz, R. E., Hyer, E. J., Kreidenweis, S. M.,
 1106 Kuciauskas, A. P., Lolli, S., Oo, M., Perry, K. D., Salinas, S. V., Sessions, W. R., Smirnov, A.,
 1107 Walker, A. L., Wang, Q., Yu, L. Y., Zhang, J. L., and Zhao, Y. J.: Aerosol meteorology of
 1108 Maritime Continent for the 2012 7SEAS southwest monsoon intensive study - Part 2: Philippine
 1109 receptor observations of fine-scale aerosol behavior, *Atmos Chem Phys*, 16, 14057-14078,
 1110 10.5194/acp-16-14057-2016, 2016b.

1111

1112 Rocha, L. D. S., and Correa, S. M.: Determination of size-segregated elements in diesel-biodiesel
 1113 blend exhaust emissions, *Environ Sci Pollut R*, 25, 18121-18129, 10.1007/s11356-018-1980-8,
 1114 2018.

1115

1116 Rogge, W. F., Mazurek, M. A., Hildemann, L. M., Cass, G. R., and Simoneit, B. R. T.:
 1117 Quantification of Urban Organic Aerosols at a Molecular-Level - Identification, Abundance and
 1118 Seasonal-Variation, *Atmos Environ a-Gen*, 27, 1309-1330, Doi 10.1016/0960-1686(93)90257-Y,
 1119 1993.

1120

1121 Ro, C. U., Oh, K. Y., Kim, H., Kim, Y. P., Lee, C. B., Kim, K. H., Kang, C. H., Osan, J., De
 1122 Hoog, J., Worobiec, A., and Van Grieken, R.: Single-particle analysis of aerosols at Cheju
 1123 Island, Korea, using low-Z electron probe X-ray microanalysis: A direct proof of nitrate
 1124 formation from sea salts, *Environ Sci Technol*, 35, 4487-4494, 10.1021/es0155231, 2001.

1125

1126 Rolph, G.D.: Real-time Environmental Applications and Display sYstem (READY) website
 1127 (<http://ready.Arl.NOAA.Gov>), NOAA Air Resour. Lab., Silver Spring, Md., 2016.

1128

1129 Roth, B., and Okada, K.: On the modification of sea-salt particles in the coastal atmosphere,
 1130 *Atmos Environ*, 32, 1555-1569, Doi 10.1016/S1352-2310(97)00378-6, 1998.

1131

1132 Saltzman, E. S., Savoie, D. L., Zika, R. G., and Prospero, J. M.: Methane Sulfonic-Acid in the
1133 Marine Atmosphere, *J Geophys Res-Oceans*, 88, 897-902, DOI 10.1029/JC088iC15p10897, 1983.
1134

1135 Saltzman, E. S., Savoie, D. L., Prospero, J. M., and Zika, R. G.: Methanesulfonic-Acid and Non-
1136 Sea-Salt Sulfate in Pacific Air - Regional and Seasonal-Variations, *J Atmos Chem*, 4, 227-240,
1137 Doi 10.1007/Bf00052002, 1986.
1138

1139 Schade, G. W., and Crutzen, P. J.: Emission of Aliphatic-Amines from Animal Husbandry and
1140 Their Reactions - Potential Source of N₂O and HCN, *J Atmos Chem*, 22, 319-346, Doi
1141 10.1007/Bf00696641, 1995.
1142

1143 Schlosser, J. S., Braun, R. A., Bradley, T., Dadashazar, H., MacDonald, A. B., Aldhaif, A. M.,
1144 Aghdam, M. A., Mardi, A. H., Xian, P., and Sorooshian, A.: Analysis of Aerosol Composition
1145 Data for Western United States Wildfires Between 2005-2015: Dust Emissions, Chloride
1146 Depletion, and Most Enhanced Aerosol Constituents, *J. Geophys. Res.*, 122,
1147 doi:10.1002/2017JD026547, 2017.
1148

1149 Schwarz, J. P., Gao, R. S., Spackman, J. R., Watts, L. A., Thomson, D. S., Fahey, D. W., Ryerson,
1150 T. B., Peischl, J., Holloway, J. S., Trainer, M., Frost, G. J., Baynard, T., Lack, D. A., de Gouw, J.
1151 A., Warneke, C., and Del Negro, L. A.: Measurement of the mixing state, mass, and optical size
1152 of individual black carbon particles in urban and biomass burning emissions, *Geophysical*
1153 *Research Letters*, 35, 10.1029/2008gl033968, 2008.
1154 Seinfeld, J. H., and Pandis, S. N.: *Atmospheric chemistry and physics* (3rd ed.). New York: Wiley-
1155 Interscience, 2016.
1156

1157 Shafer, M. M., Toner, B. M., Oyerdier, J. T., Schauer, J. J., Fakra, S. C., Hu, S. H., Herner, J. D.,
1158 and Ayala, A.: Chemical Speciation of Vanadium in Particulate Matter Emitted from Diesel
1159 Vehicles and Urban Atmospheric Aerosols, *Environ Sci Technol*, 46, 189-195,
1160 10.1021/es200463c, 2012.
1161

1162 Shingler, T., Sorooshian, A., Ortega, A., Crosbie, E., Wonaschutz, A., Perring, A. E.,
1163 Beyersdorf, A., Ziemba, L., Jimenez, J. L., Campuzano-Jost, P., Mikoviny, T., Wisthaler, A., and
1164 Russell, L. M.: Ambient observations of hygroscopic growth factor and f(RH) below 1: Case
1165 studies from surface and airborne measurements, *J Geophys Res-Atmos*, 121, 13661-13677,
1166 10.1002/2016jd025471, 2016.
1167

1168 Shiraiwa, M., Kondo, Y., Moteki, N., Takegawa, N., Sahu, L. K., Takami, A., Hatakeyama, S.,
1169 Yonemura, S., and Blake, D. R.: Radiative impact of mixing state of black carbon aerosol in Asian
1170 outflow, *Journal of Geophysical Research: Atmospheres*, 113, 10.1029/2008jd010546, 2008.
1171

1172 Simpas, J., Lorenzo, G., and Cruz, M. T.: Monitoring Particulate Matter Levels and Composition
1173 for Source Apportionment Study in Metro Manila, Philippines, in: *Improving Air Quality in Asian*
1174 *Developing Countries: Compilation of Research Findings*, Kim Oanh, N. T. (Ed.), NARENCA,
1175 Vietnam Publishing House of Natural Resources, Environment and Cartography, Vietnam, 239-
1176 261, 2014.
1177

1178 Singh, M., Jaques, P. A., and Sioutas, C.: Size distribution and diurnal characteristics of particle-
1179 bound metals in source and receptor sites of the Los Angeles Basin, *Atmos Environ*, 36, 1675-
1180 1689, Pii S1352-2310(02)00166-8, Doi 10.1016/S1352-2310(02)00166-8, 2002.

1181

1182 Song, F., and Gao, Y.: Size distributions of trace elements associated with ambient particular
1183 matter in the affinity of a major highway in the New Jersey-New York metropolitan area, *Atmos*
1184 *Environ*, 45, 6714-6723, 10.1016/j.atmosenv.2011.08.031, 2011.

1185

1186 Sorooshian, A., Ng, N. L., Chan, A. W. H., Feingold, G., Flagan, R. C., and Seinfeld, J. H.:
1187 Particulate organic acids and overall water-soluble aerosol composition measurements from the
1188 2006 Gulf of Mexico Atmospheric Composition and Climate Study (GoMACCS), *J Geophys*
1189 *Res-Atmos*, 112, 10.1029/2007jd008537, 2007.

1190

1191 Sorooshian, A., Murphy, S. N., Hersey, S., Gates, H., Padro, L. T., Nenes, A., Brechtel, F. J.,
1192 Jonsson, H., Flagan, R. C., and Seinfeld, J. H.: Comprehensive airborne characterization of aerosol
1193 from a major bovine source, *Atmos Chem Phys*, 8, 5489-5520, DOI 10.5194/acp-8-5489-2008,
1194 2008.

1195

1196 Sorooshian, A., Padro, L. T., Nenes, A., Feingold, G., McComiskey, A., Hersey, S. P., Gates, H.,
1197 Jonsson, H. H., Miller, S. D., Stephens, G. L., Flagan, R. C., and Seinfeld, J. H.: On the link
1198 between ocean biota emissions, aerosol, and maritime clouds: Airborne, ground, and satellite
1199 measurements off the coast of California, *Global Biogeochem Cy*, 23,
1200 10.1029/2009gb003464, 2009.

1201

1202 Sorooshian, A., Crosbie, E., Maudlin, L. C., Youn, J. S., Wang, Z., Shingler, T., Ortega, A. M.,
1203 Hersey, S., and Woods, R. K.: Surface and airborne measurements of organosulfur and
1204 methanesulfonate over the western United States and coastal areas, *J Geophys Res-Atmos*, 120,
1205 8535-8548, 10.1002/2015jd023822, 2015.

1206

1207 Stein, A. F., Draxler, R. R., Rolph, G. D., Stunder, B. J. B., Cohen, M. D., and Ngan, F.: NOAA's
1208 Hysplit Atmospheric Transport and Dispersion Modeling System, *B Am Meteorol Soc*, 96, 2059-
1209 2077, 10.1175/Bams-D-14-00110.1, 2015.

1210

1211 Tai, A. P. K., Mickley, L. J., and Jacob, D. J.: Correlations between fine particulate matter (PM_{2.5})
1212 and meteorological variables in the United States: Implications for the sensitivity of PM_{2.5} to
1213 climate change, *Atmos Environ*, 44, 3976-3984, 10.1016/j.atmosenv.2010.06.060, 2010.

1214

1215 Tsakalou, C., Papamarkou, S., Tsakiridis, P. E., Bartzas, G., and Tsakalakis, K.: Characterization
1216 and leachability evaluation of medical wastes incineration fly and bottom ashes and their
1217 vitrification outgrowths, *J Environ Chem Eng*, 6, 367-376, 10.1016/j.jece.2017.12.012, 2018.

1218

1219 U.S. Environmental Protection Agency: Monitoring PM_{2.5} in Ambient Air
1220 Using Designated Reference or Class I Equivalent Methods. Report No. EPA-454/B-16-001. US
1221 Environmental Protection Agency, Research Triangle Park, NC., 2016.

1222

1223 VandenBoer, T. C., Petroff, A., Markovic, M. Z., and Murphy, J. G.: Size distribution of alkyl
1224 amines in continental particulate matter and their online detection in the gas and particle phase,
1225 Atmos Chem Phys, 11, 4319-4332, 10.5194/acp-11-4319-2011, 2011.
1226
1227 Villafuerte, M. Q., Matsumoto, J., Akasaka, I., Takahashi, H. G., Kubota, H., and Cinco, T. A.:
1228 Long-term trends and variability of rainfall extremes in the Philippines, Atmos Res, 137, 1-13,
1229 10.1016/j.atmosres.2013.09.021, 2014.
1230
1231 Vossler, T., Cernikovskiy, L., Novak, J., and Williams, R.: Source apportionment with
1232 uncertainty estimates of fine particulate matter in Ostrava, Czech Republic using Positive Matrix
1233 Factorization, Atmos Pollut Res, 7, 503-512, 10.1016/j.apr.2015.12.004, 2016.
1234
1235 Wang, J., Ge, C., Yang, Z. F., Hyer, E. J., Reid, J. S., Chew, B. N., Mahmud, M., Zhang, Y. X.,
1236 and Zhang, M. G.: Mesoscale modeling of smoke transport over the Southeast Asian Maritime
1237 Continent: Interplay of sea breeze, trade wind, typhoon, and topography, Atmos Res, 122, 486-
1238 503, 10.1016/j.atmosres.2012.05.009, 2013.
1239
1240 Wang, Y. Q., Zhang, X. Y., and Draxler, R. R.: TrajStat: GIS-based software that uses various
1241 trajectory statistical analysis methods to identify potential sources from long-term air pollution
1242 measurement data, Environ Modell Softw, 24, 938-939, 10.1016/j.envsoft.2009.01.004, 2009.
1243
1244 Wasson, S. J., Linak, W. P., Gullett, B. K., King, C. J., Touati, A., Huggins, F. E., Chen, Y. Z.,
1245 Shah, N., and Huffman, G. P.: Emissions of chromium, copper, arsenic, and PCDDs/Fs from open
1246 burning of CCA-treated wood, Environ Sci Technol, 39, 8865-8876, 10.1021/es050891g, 2005.
1247
1248 Watson, J. G.: Protocol for Applying and Validating the CMB Model for PM_{2.5} and VOC. Report
1249 No. EPA-451/R-04-001. US Environmental Protection Agency, Research Triangle Park, NC.,
1250 2004.
1251
1252 Watts, S. F., Watson, A., and Brimblecombe, P.: Measurements of the Aerosol Concentrations of
1253 Methanesulfonic Acid, Dimethyl-Sulfoxide and Dimethyl Sulfone in the Marine Atmosphere of
1254 the British-Isles, Atmos Environ, 21, 2667-2672, Doi 10.1016/0004-6981(87)90198-3, 1987.
1255
1256 Wonaschuetz, A., Sorooshian, A., Ervens, B., Chuang, P. Y., Feingold, G., Murphy, S. M., de
1257 Gouw, J., Warneke, C., and Jonsson, H. H.: Aerosol and gas re-distribution by shallow cumulus
1258 clouds: An investigation using airborne measurements, J Geophys Res-Atmos, 117,
1259 10.1029/2012jd018089, 2012.
1260
1261 Wu, D., Zhang, F., Lou, W. H., Li, D., and Chen, J. M.: Chemical characterization and toxicity
1262 assessment of fine particulate matters emitted from the combustion of petrol and diesel fuels, Sci
1263 Total Environ, 605, 172-179, 10.1016/j.scitotenv.2017.06.058, 2017.
1264
1265 Xian, P., Reid, J. S., Atwood, S. A., Johnson, R. S., Hyer, E. J., Westphal, D. L., and Sessions, W.:
1266 Smoke aerosol transport patterns over the Maritime Continent, Atmos Res, 122, 469-485,
1267 10.1016/j.atmosres.2012.05.006, 2013.
1268

1269 Xu, G. J., and Gao, Y.: Characterization of marine aerosols and precipitation through shipboard
1270 observations on the transect between 31 degrees N-32 degrees S in the West Pacific, *Atmos Pollut*
1271 *Res*, 6, 154-161, 10.5094/Apr.2015.018, 2015.

1272

1273 Yao, X. H., Fang, M., and Chan, C. K.: The size dependence of chloride depletion in fine and
1274 coarse sea-salt particles, *Atmos Environ*, 37, 743-751, 10.1016/S1352-2310(02)00955-X, 2003.

1275

1276 Youn, J. S., Wang, Z., Wonaschutz, A., Arellano, A., Betterton, E. A., and Sorooshian, A.:
1277 Evidence of aqueous secondary organic aerosol formation from biogenic emissions in the North
1278 American Sonoran Desert, *Geophys Res Lett*, 40, 3468-3472, 10.1002/grl.50644, 2013.

1279

1280 Youn, J. S., Crosbie, E., Maudlin, L. C., Wang, Z., and Sorooshian, A.: Dimethylamine as a major
1281 alkyl amine species in particles and cloud water: Observations in semi-arid and coastal regions,
1282 *Atmos Environ*, 122, 250-258, 10.1016/j.atmosenv.2015.09.061, 2015.

1283

1284 Youn, J. S., Csavina, J., Rine, K. P., Shingler, T., Taylor, M. P., Saez, A. E., Betterton, E. A., and
1285 Sorooshian, A.: Hygroscopic Properties and Respiratory System Deposition Behavior of
1286 Particulate Matter Emitted By Mining and Smelting Operations, *Environ Sci Technol*, 50, 11706-
1287 11713, 10.1021/acs.est.6b03621, 2016.

1288

1289 **Table 1.** Summary of average operating parameters, meteorological conditions, and total resolved
 1290 water-soluble mass concentration for each MOUDI sample set collected at Manila Observatory
 1291 (MO) during the 2018 Southwest Monsoon period. On two occasions, simultaneous MOUDI sets
 1292 were collected for one set to undergo gravimetric analysis (MO3 and MO13) to compare with mass
 1293 resolved from chemical speciation of the water-soluble fraction (MO4 and MO14). One additional
 1294 MOUDI set devoted to microscopy analysis was collected using aluminum substrates for one hour
 1295 on August 1 at 30 LPM.
 1296

Sample set name	Dates	Duratio ion (hrs)	Flow rate (LPM)	Wind speed (m/s)	Wind direction (°)	T (°C)	Rain (mm)	Water- soluble mass ($\mu\text{g m}^{-3}$)
MO1	Jul 19-20	24	30	3.3	90.1	24.9	47	4.6
MO2	Jul 23-25	54	30	1.3	95.8	26.7	7.8	6.5
MO3/4	Jul 25-30	119	28/30	1.2	111.8	26.7	49.6	5.2
MO5	Jul 30-Aug 1	42	29	2.6	98.1	27.5	52.8	9.2
MO6	Aug 6-8	48	27	0.9	127.5	26.1	30.4	5.1
MO7	Aug 14-16	48	28	3.0	107.8	27.8	2.8	13.7
MO8	Aug 22-24	48	29	3.5	108.7	28.1	1	12.8
MO9	Sep 1-3	48	27	0.7	98.6	26.6	51.6	6.2
MO10	Sep 10-12	48	29	1.0	94.7	26.2	78.4	6.4
MO11	Sep 18-20	48	27	0.5	290.2	27.8	0	2.7
MO12	Sep 26-28	48	27	1.2	96.3	27.8	6.8	13.5
MO13/14	Oct 6-8	48	28/26	0.6	108.2	27.8	0.8	16.6

1297
 1298

1299 **Table 2.** Charge balance slopes (cations on y-axis; anions on x-axis) for the MOUDI sets shown
 1300 including the averages of all sets (All) for three size ranges: submicrometer stages spanning 0.056
 1301 – 1.0 μm ; supermicrometer stages ($> 1.0 \mu\text{m}$); and all stages ($> 0.056 \mu\text{m}$). The species used in
 1302 the charge balance analysis include those speciated with the IC (listed in Section 2.3) plus K from
 1303 ICP-QQQ analysis.
 1304

Sample set	0.056 – 1.0 μm	$> 1 \mu\text{m}$	$> 0.056 \mu\text{m}$
MO1	0.87	1.37	0.89
MO2	1.46	1.26	1.41
MO4	1.25	1.17	1.21
MO5	1.35	1.43	1.41
MO6	1.29	1.45	1.31
MO7	1.40	1.23	1.36
MO8	1.35	1.33	1.36
MO9	1.28	1.55	1.26
MO10	1.37	1.36	1.35
MO11	0.97	1.60	1.27
MO12	1.37	1.19	1.33
MO14	1.31	1.28	1.29
All	1.35	1.24	1.33

1305
 1306

1307 **Table 3.** Contributions (in weight percentage) of each PMF source factor to the total mass in
 1308 different diameter ranges.
 1309

Diameter Range (μm)	Aged/Transported	Sea Salt	Combustion	Vehicular/Resuspended Dust	Waste Processing
> 0.056	48.0%	22.5%	18.7%	5.6%	5.1%
0.056 - 1.0	68.9%	0.6%	23.9%	1.5%	5.1%
> 1.0	18.6%	53.5%	11.3%	11.3%	5.3%

1310

1311 **Table 4.** Correlation matrix (r values) between water-soluble species based on total MOUDI-
 1312 integrated mass concentrations (> 0.056 μm). Blank cells represent statistically insignificant
 1313 values. Results for the sub- and supermicrometer ranges are in Tables S2-S3. Panels A-E
 1314 represent important species from each of the source profiles identified in Section 3.3: A = Aged,
 1315 B = Sea Salt, C = Combustion, D = Vehicular/Resuspended Dust, E = Waste Processing. DMA –
 1316 Dimethylamine, MSA – Methanesulfonate, PH – Phthalate, OX – Oxalate, MA – Maleate, SU –
 1317 Succinate, AD – Adipate.
 1318

A)																
OX	1.00															
SO₄	0.74	1.00														
NH₄	0.68	0.99	1.00													
Sn	0.71	0.87	0.85	1.00												
Rb	0.73	0.74	0.73	0.69	1.00											
K	0.76	0.71	0.69	0.69	0.97	1.00										
Cs	0.72	0.82	0.81	0.74	0.96	0.91	1.00									
V	0.36	0.64	0.63	0.48	0.53	0.51	0.57	1.00								
DMA		0.35		0.38	0.45	0.37	0.45		1.00							
MSA	0.71	0.89	0.89	0.79	0.90	0.85	0.92	0.51	0.47	1.00						
PH	0.68	0.67	0.68	0.73	0.82	0.76	0.80		0.38	0.88	1.00					
SU	0.63	0.56	0.59	0.44	0.87	0.81	0.82		0.68	0.78	0.84	1.00				
AD	0.40	0.66	0.70	0.62	0.70	0.70	0.77		0.84	0.74	0.75	0.90	1.00			
Se	0.75	0.75	0.73	0.66	0.80	0.78	0.79	0.32	0.34	0.78	0.80	0.88	0.88	1.00		
Tl	0.75	0.87	0.86	0.80	0.89	0.85	0.94	0.74	0.65	0.80	0.52	0.70		0.43	1.00	
	OX	SO₄	NH₄	Sn	Rb	K	Cs	V	DMA	MSA	PH	SU	AD	Se	Tl	

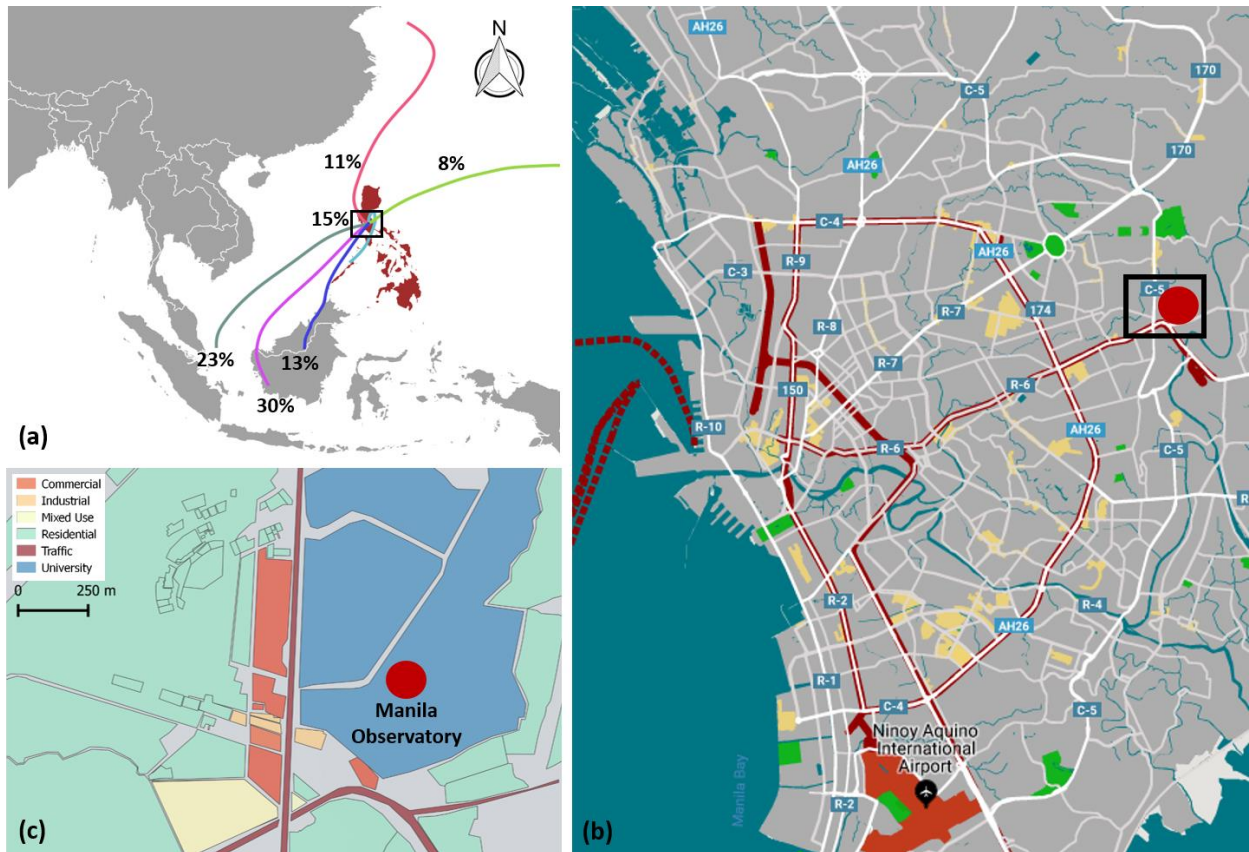
B)								
Cl	1.00							
NO₃	0.76	1.00						
Ba	0.66	0.80	1.00					
Sr	0.78	0.87	0.91	1.00				
Ca	0.58	0.79	0.75	0.78	1.00			
Na	0.93	0.87	0.75	0.85	0.63	1.00		
Mg	0.91	0.87	0.77	0.87	0.66	0.99	1.00	
Hf					0.57			1.00
	Cl	NO₃	Ba	Sr	Ca	Na	Mg	Hf

C)								
As	1.00							
Ni	0.58	1.00						
Co			1.00					
P		0.33	0.34	1.00				
Mo					1.00			
Cr	0.62	0.49		0.20		1.00		
MA			0.67		-0.42		1.00	
Ag			0.85		0.64			1.00
	As	Ni	Co	P	Mo	Cr	Mal	Ag

D)						
Zr	1.00					
Y	0.75	1.00				
Al	0.88	0.76	1.00			
Fe	0.33	0.61	0.25	1.00		
Ti	0.84	0.66	0.82	0.41	1.00	
Nb	0.70	0.50	0.59	0.59	0.70	1.00
	Zr	Y	Al	Fe	Ti	Nb

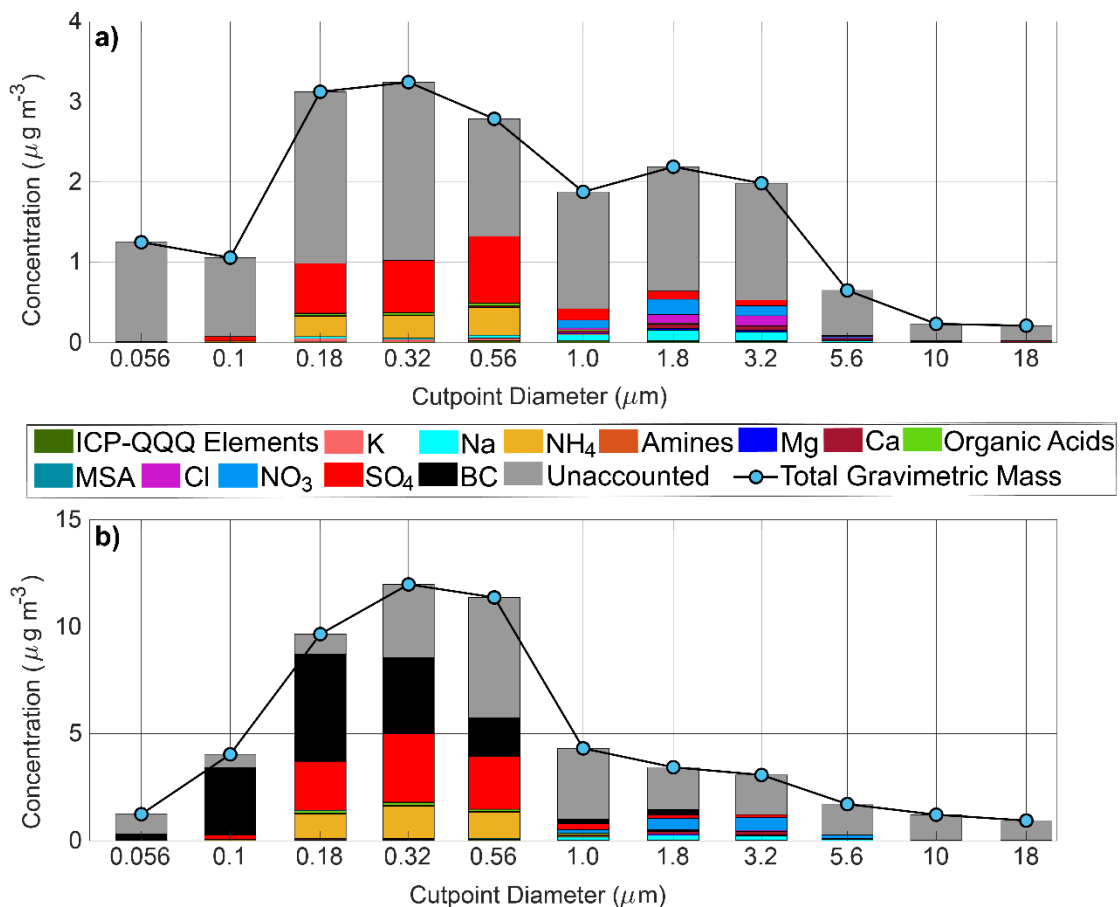
E)					
Cd	1.00				
Zn	0.60	1.00			
Cu	0.21	0.27	1.00		
Mn	0.28	0.61	0.22	1.00	
Pb	0.78	0.58	0.38	0.27	1.00
	Cd	Zn	Cu	Mn	Pb

1319
 1320
 1321
 1322



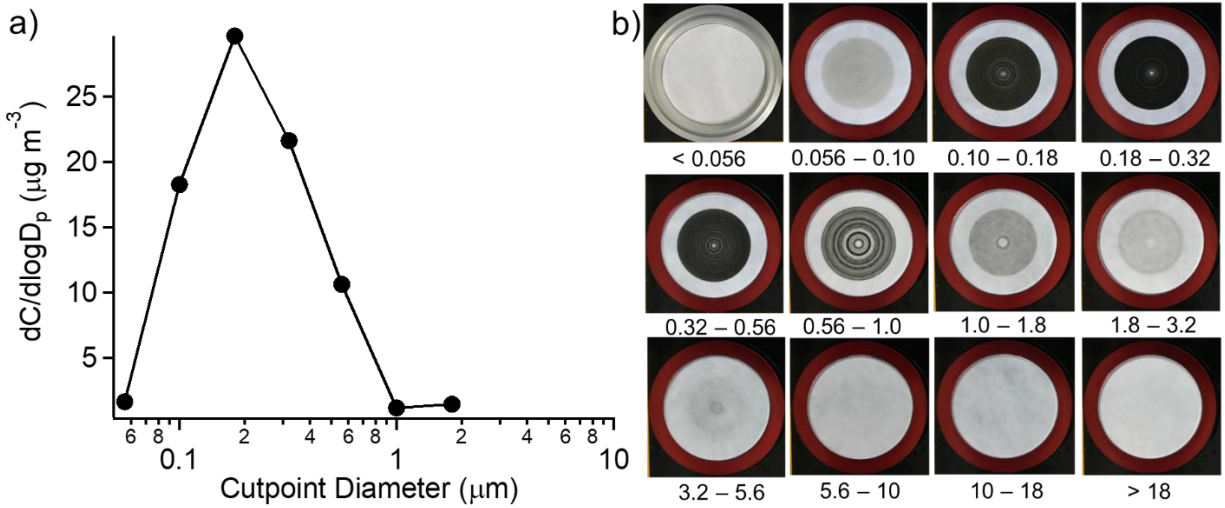
1323
 1324 **Figure 1.** (a) Location of Metro Manila, Philippines relative to Southeast Asia. Also shown are
 1325 5-day backward trajectory frequencies during the sampling duration based on HYSPLIT cluster
 1326 analysis; note that 15% correspond to trajectories within the black square. (b) Close-up view of
 1327 Metro Manila showing the location of the Manila Observatory sampling site with a black rectangle.
 1328 The base map shows roads, commercial centers, and major transit lines in the city. (c) Land use
 1329 classification in the vicinity of the sampling site. (Sources: GADM, Snazzy Maps, OpenStreetMap,
 1330 NOAA HYSPLIT, & TrajSat)

1331
 1332
 1333
 1334
 1335
 1336



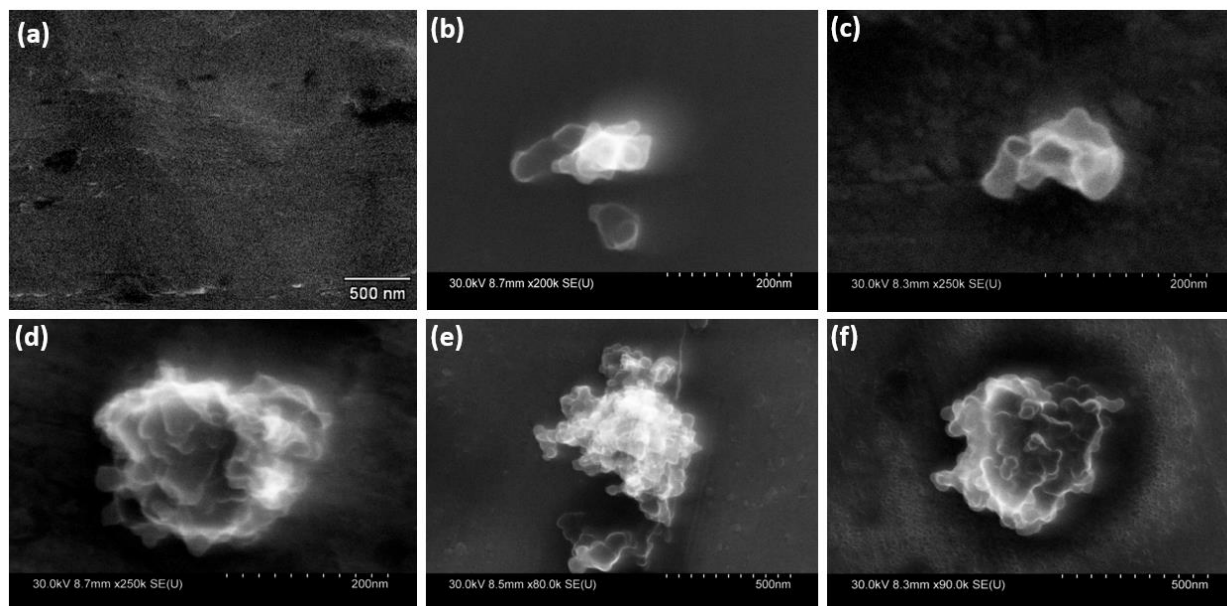
1337
 1338 **Figure 2.** Mass size distributions of total PM (blue markers) and resolved chemical species
 1339 (colored bars) for MOUDI sets (a) MO3/4 and (b) MO13/14. Note that set MO13 was the single
 1340 MOUDI set where BC was quantified. ICP-QQQ = sum of water-soluble elements except K;
 1341 amines = sum of DMA, TMA, DEA; organic acids = sum of oxalate, succinate, adipate,
 1342 pyruvate, phthalate, maleate.
 1343

1344



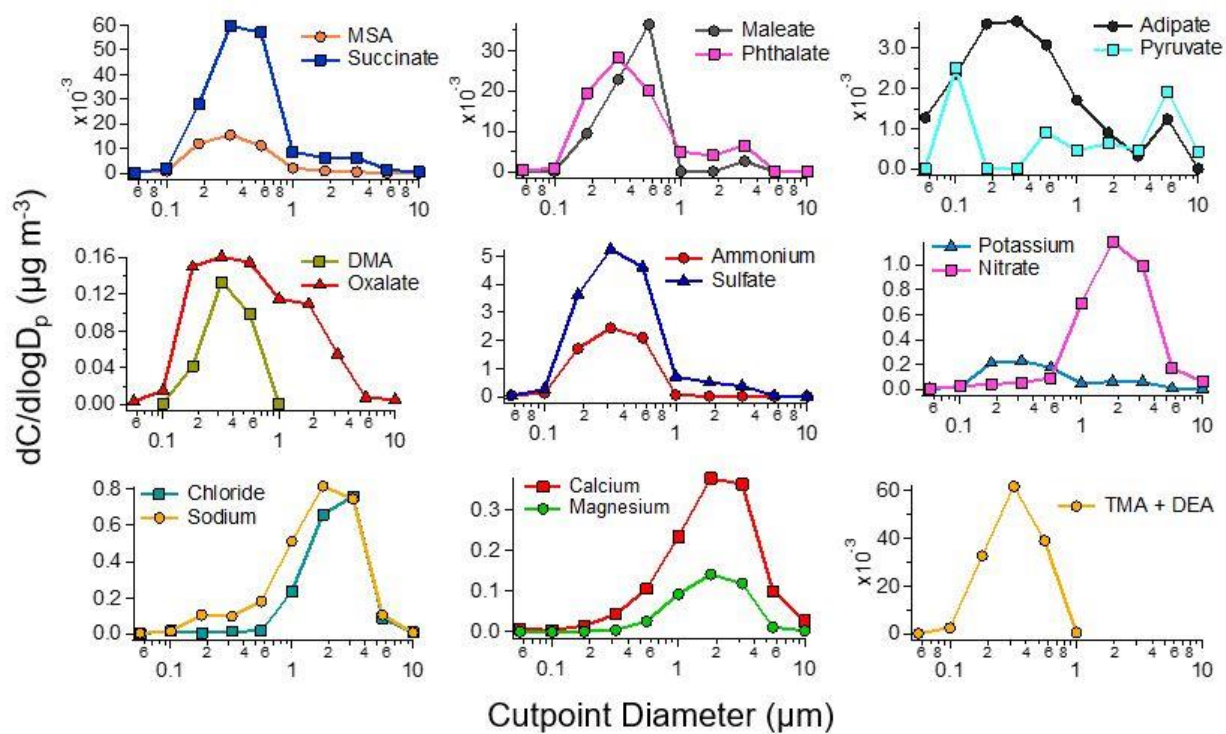
1345
1346
1347
1348
1349
1350

Figure 3. (a) Mass size distribution of BC retrieved from the MABI optical measurement at 870 nm for set MO13. Missing values were below detection limits. (b) Photographs of each stage of set MO13 with numbers below each image representing the aerodynamic diameter ranges in units of μm .



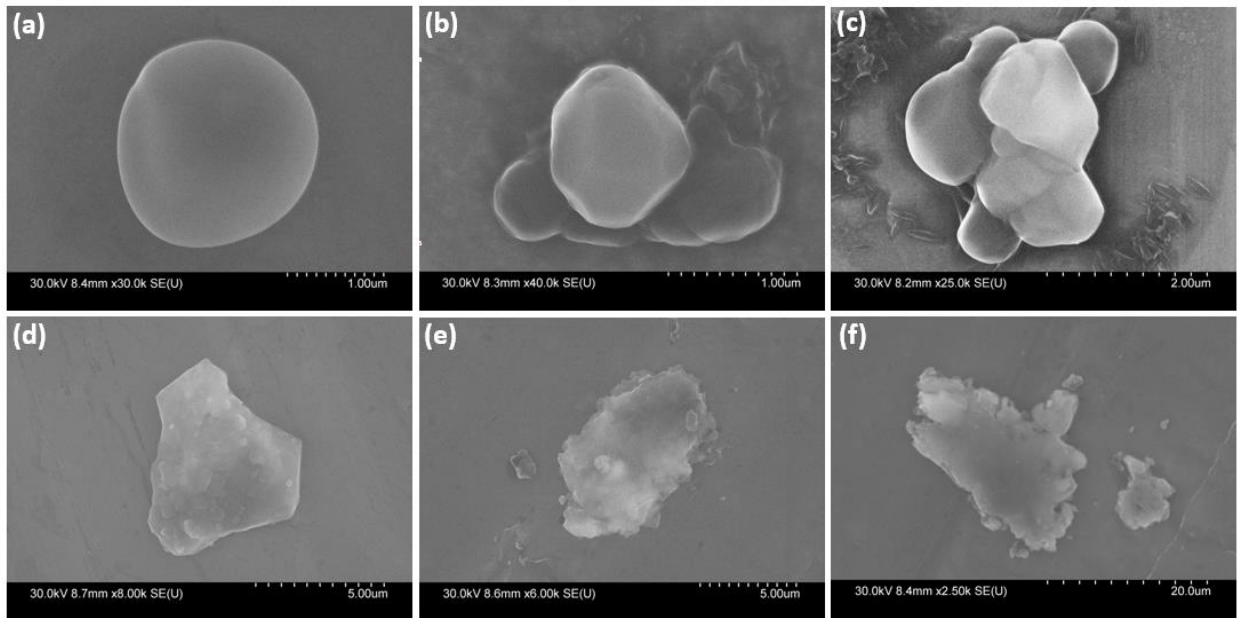
1351
1352
1353
1354
1355

Figure 4. SEM image of a (a) blank filter and (b-f) individual particles in different sub-micrometer aerodynamic diameter ranges sampled by the MOUDI: (b) 0.056–0.1 μm , (c) 0.1–0.18 μm , (d) 0.18–0.32 μm , (e) 0.32–0.56 μm , (f) 0.56–1.0 μm .



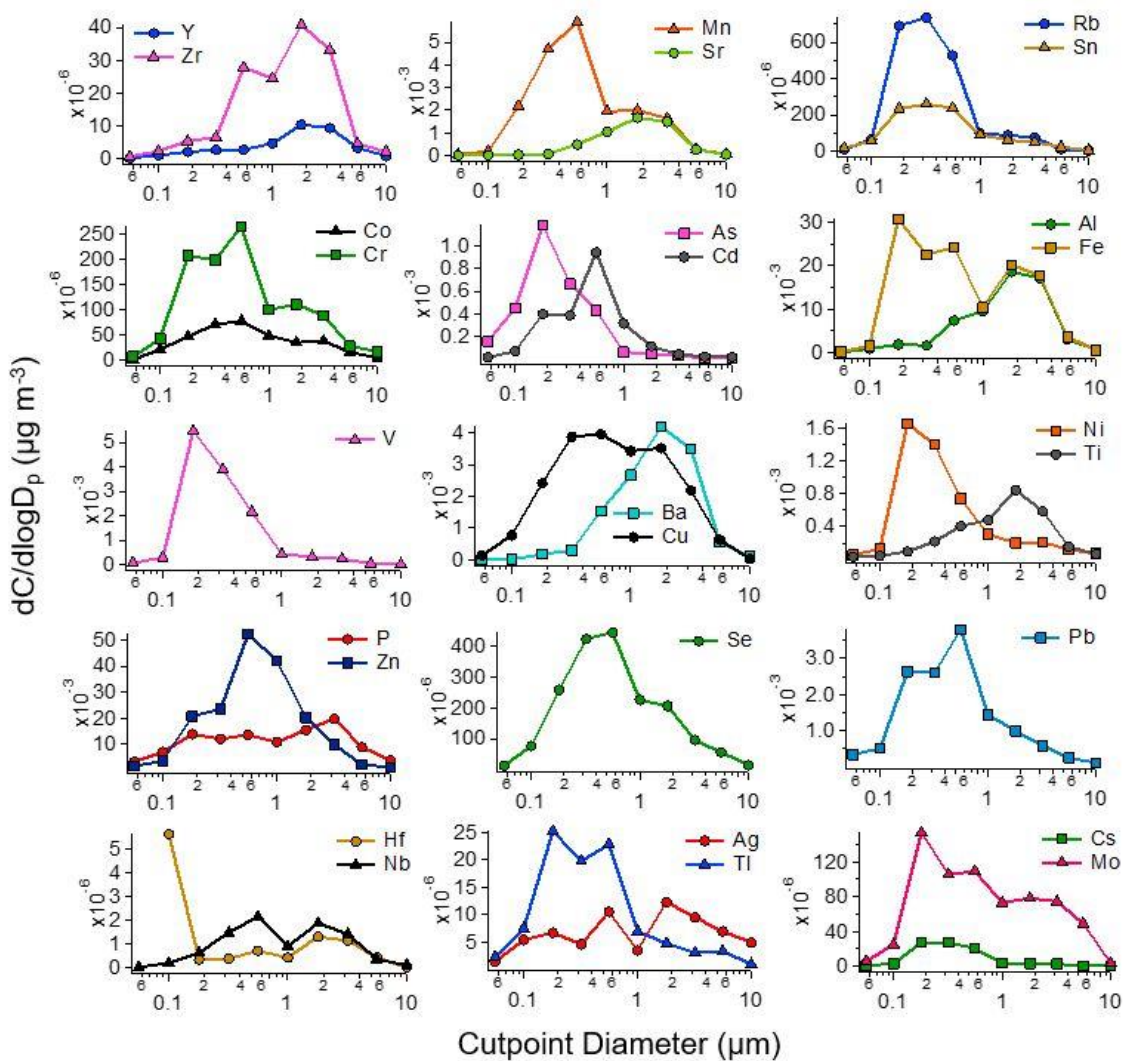
1356
 1357 **Figure 5.** Average mass size distribution of water-soluble ions speciated via IC in addition to
 1358 potassium from ICP-QQQ analysis.
 1359

1360



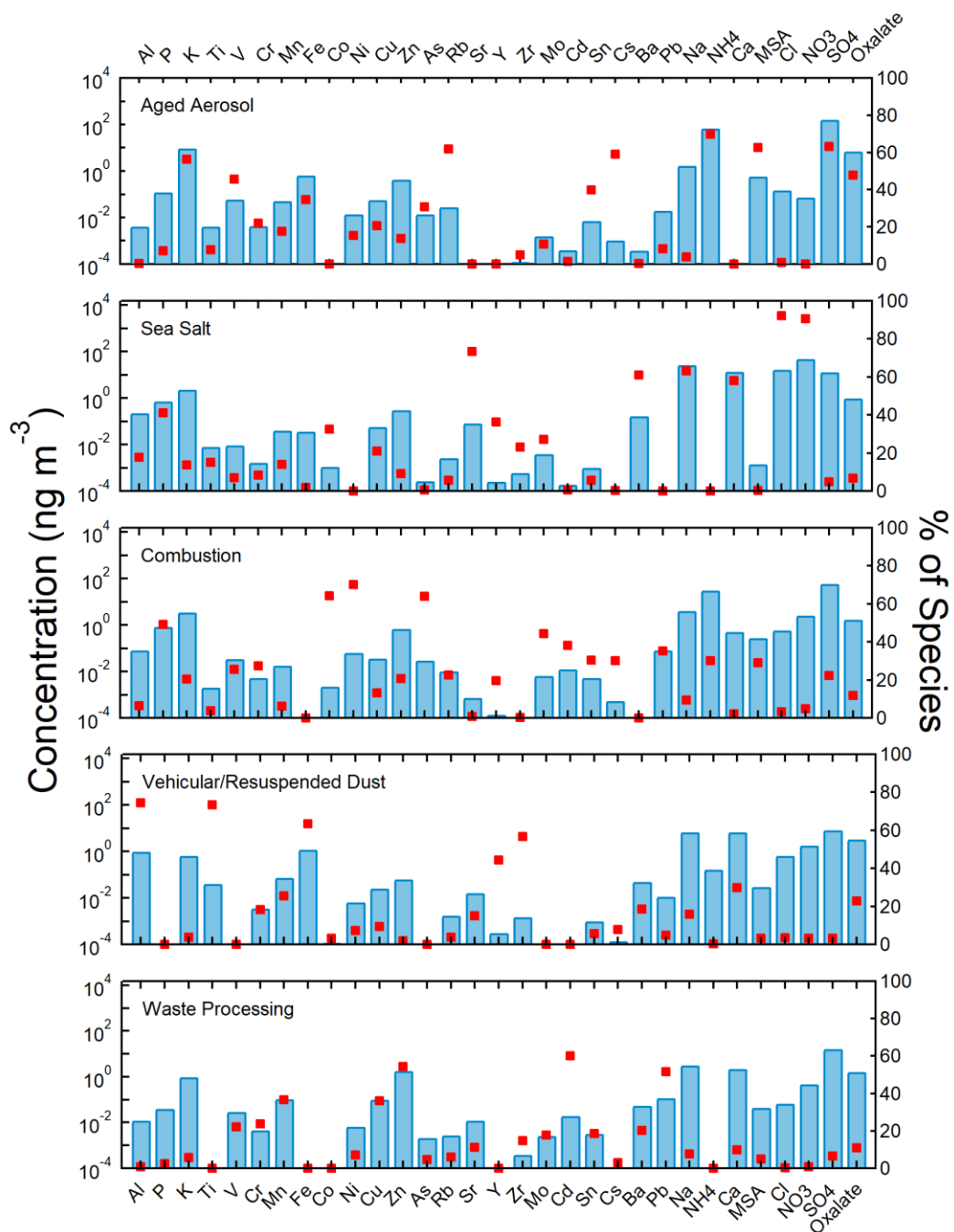
1361
1362
1363
1364
1365

Figure 6. Same as Figure 4, but for different supermicrometer aerodynamic diameter ranges sampled by the MOUDI: (a) 1.0–1.8 μm , (b) 1.8–3.2 μm ; (c) 3.2–5.6 μm , (d) 5.6–10 μm , (e) 10–18 μm , (f) > 18 μm .

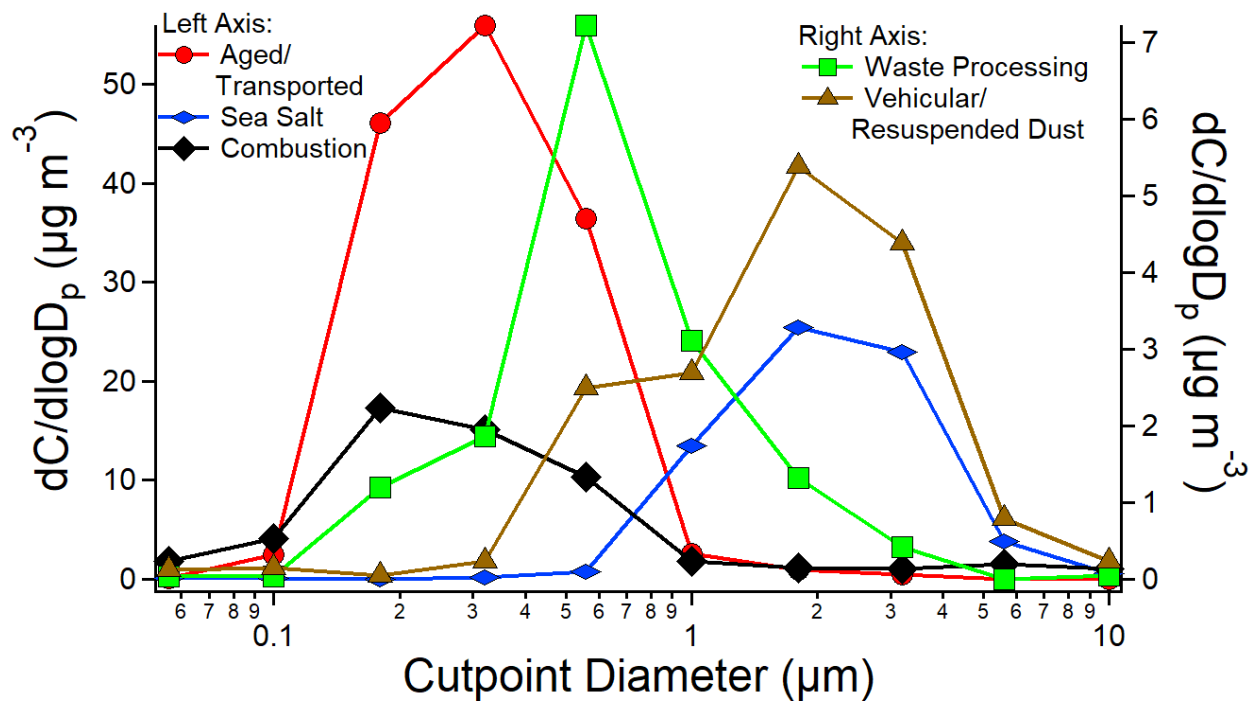


1366
 1367
 1368
 1369

Figure 7. Average mass size distribution of water-soluble elements speciated via ICP-QQQ.



1370
 1371 **Figure 8.** Overview of the PMF five factor solution with blue bars representing mass
 1372 concentrations and red squares signifying the percentage of mass concentration contributed to
 1373 constituents by each source factor.
 1374



1375
 1376
 1377

Figure 9. Reconstructed mass size distributions using PMF for the five major source profiles.